NAVAL AIR WARFARE CENTER AIRCRAFT DIVISION
PATUXENT RIVER, MARYLAND

TECHNICAL REPORT

REPORT NO: NAWCADPAX/TR-2009/12

AIRCRAFT STEELS

by

E. U. Lee
R. Taylor
C. Lei
H. C. Sanders

19 February 2009

Approved for public release; distribution is unlimited.

DEPARTMENT OF THE NAVY
NAVAL AIR WARFARE CENTER AIRCRAFT DIVISION
PATUXENT RIVER, MARYLAND

NAWCADPAX/TR-2009/12
19 February 2009

AIRCRAFT STEELS

by

E. U. Lee
R. Taylor
C. Lei
H. C. Sanders

RELEASED BY:

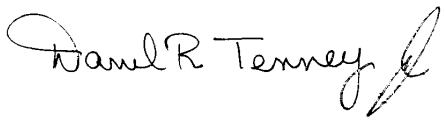

19 Feb 2009

DARREL TENNEY, JR. / AIR-4.3.4 / DATE
Division Head, Materials Engineering Division
Naval Air Warfare Center Aircraft Division

REPORT DOCUMENTATION PAGE

Form Approved
OMB No. 0704-0188

Public reporting burden for this collection of information is estimated to average 1 hour per response, including the time for reviewing instructions, searching existing data sources, gathering and maintaining the data needed, and completing and reviewing this collection of information. Send comments regarding this burden estimate or any other aspect of this collection of information, including suggestions for reducing this burden, to Department of Defense, Washington Headquarters Services, Directorate for Information Operations and Reports (0704-0188), 1215 Jefferson Davis Highway, Suite 1204, Arlington, VA 22202-4302. Respondents should be aware that notwithstanding any other provision of law, no person shall be subject to any penalty for failing to comply with a collection of information if it does not display a currently valid OMB control number. PLEASE DO NOT RETURN YOUR FORM TO THE ABOVE ADDRESS.

1. REPORT DATE	2. REPORT TYPE	3. DATES COVERED
19 February 2009	Technical Report	

4. TITLE AND SUBTITLE	5a. CONTRACT NUMBER
Aircraft Steels	5b. GRANT NUMBER
	5c. PROGRAM ELEMENT NUMBER

6. AUTHOR(S)	5d. PROJECT NUMBER
E. U. Lee R. Taylor C. Lei H. C. Sanders	5e. TASK NUMBER
	5f. WORK UNIT NUMBER

7. PERFORMING ORGANIZATION NAME(S) AND ADDRESS(ES)	8. PERFORMING ORGANIZATION REPORT NUMBER
Naval Air Warfare Center Aircraft Division 22347 Cedar Point Road, Unit #6 Patuxent River, Maryland 20670-1161	NAWCADPAX/TR-2009/12

9. SPONSORING/MONITORING AGENCY NAME(S) AND ADDRESS(ES)	10. SPONSOR/MONITOR'S ACRONYM(S)
Naval Air Systems Command 47123 Buse Road Unit IPT Patuxent River, Maryland 20670-1547	11. SPONSOR/MONITOR'S REPORT NUMBER(S)

12. DISTRIBUTION/AVAILABILITY STATEMENT

Approved for public release; distribution is unlimited.

13. SUPPLEMENTARY NOTES

14. ABSTRACT

Five high strength steels (4340, 300M, AerMet 100, Ferrium S53, and Hy-Tuf) and four stainless steels (High Nitrogen, 13-8Mo, Custom 465, and MLX17) have been evaluated with respect to their characteristics and applicability to the current and future Navy aircraft. In this endeavor, their metallurgical feature, mechanical property, fatigue behavior, and corrosion resistance have been investigated and compared.

15. SUBJECT TERMS

4340, 300M, AerMet 100, Ferrium S53, Hy-Tuf, high strength steels, stainless steels

16. SECURITY CLASSIFICATION OF:			17. LIMITATION OF ABSTRACT	18. NUMBER OF PAGES	19a. NAME OF RESPONSIBLE PERSON
a. REPORT	b. ABSTRACT	c. THIS PAGE			19b. TELEPHONE NUMBER (include area code)
Unclassified	Unclassified	Unclassified	SAR	46	Eun Lee 301-342-8069

Standard Form 298 (Rev. 8-98)
Prescribed by ANSI Std. Z39-18

SUMMARY

Five high strength and four stainless steels have been studied, identifying their microstructural feature, determining their mechanical property, examining their fatigue behavior in different environments, and investigating their stress corrosion cracking. The results of this study indicate that the high strength steels need better corrosion resistance and the stainless steels need greater mechanical property for their optimum usage in the current and future aircraft.

Contents

Page No.

Introduction 1

Experimental Procedure 2
- Material and Heat Treatment 2
- Specimen 3
- Tests 3

Results and Discussion 5
- Mechanical Properties 5
- Fatigue Behavior 5
  - Stress-Life Fatigue on High Strength and Stainless Steels 5
  - Fatigue Crack Growth in High Strength Steels 5
  - Variation of Fatigue Crack Growth/Time, da/dt, with Maximum Stress Intensity, K_{max}, in High Strength Steels 6
  - Fatigue Crack Growth in Stainless Steels 7
- Fractographic Features 8
  - High Strength Steels 8
  - Stainless Steels 9

Conclusions 10

Recommendations 10

References 11

Appendices
- A. Figures 13
- B. Tables 14

Distribution 15

ACKNOWLEDGEMENT

The authors would like to thank Mr. Joe Bilko for specimen preparation.

INTRODUCTION

For structural components, 4340, 300M, AerMet 100, and Hy-Tuf steels have been widely used. 4340 steel, developed in 1940's, is a low alloy steel with good hardenability. In 1950's, this steel was modified to 300M steel, having somewhat higher strength but low fracture toughness K_{IC}, 57 MPa√m (52 ksi√in.). Subsequently, AF1410 steel was developed to have a higher K_{IC}, 181 MPa√m (165 ksi√in.). However, its ultimate tensile strength (UTS) is only 1,669 MPa (242 ksi), not suitable for highly stressed structural component. In the early 1990's, a new Co-Ni alloy steel, AerMet 100 steel, was developed. It has an outstanding combination of high UTS, 1,979 MPa (294 ksi), and high K_{IC}, exceeding 110 MPa√m (100 ksi√in.). Therefore, AerMet 100 steel has been used more and more for aircraft and other structural components. However, its corrosion resistance is low and susceptible to stress corrosion cracking (SCC). Therefore, a new generation steel with better SCC resistance, Ferrium S53, has been emerged in 2002. This provides high UTS 1,986 MPa (288 ksi) and K_{ISCC} 38 MPa√m (35 ksi) √in., but low yield strength (YS) 1,572 MPa (228 ksi). Hy-Tuf is a low alloy high strength steel, which was developed to exceed a strength of 1,379 MPa (200 ksi). This steel has a relatively high impact strength and low notch sensitivity with good ductility.

High strength steels with high corrosion resistance have been under development more or less continuously since 1960's. The metallurgical base for such steels has been a martensitic matrix of low C concentration. The intrinsic brittleness has been mitigated by tempering with proper combinations of temperature and time. In these steels, 12 – 14% Cr is incorporated to have high corrosion resistance. In combination with the large concentrations of many different alloying elements present, the small C concentration provides good hardenability. Among those stainless steels, PH 13-8Mo, Custom 465 and MLX17 are considered for the current and future structural component usage. PH 13-8Mo is a precipitation-hardenable martensitic stainless steel combining excellent corrosion resistance with strength. Custom 465 is a martensitic, age-hardenable stainless steel capable of about 1,724 MPa (250 ksi) UTS when peak-aged (H900 condition). Especially, this steel can be readily cold-formed by drawing or rolling. Single step aging of cold-worked steel results in enhanced strengthening. MLX17 is a stainless steel recently developed in France. It has good mechanical properties and high SCC resistance.

On the other hand, the high nitrogen stainless steel (HNSS) is an austenitic stainless steel, which offers an excellent corrosion resistance and a high work-hardenability. Alloying with N in solid solution confers particularly interesting properties on these steels: it stabilizes the face centered cubic lattice and enhances the resistance to pitting corrosion, intergranular corrosion and SCC. In addition, the N alloying enhances YS and UTS, and improves creep and fatigue resistance, as well as maintaining the high toughness. These effects, together with the grain refinement and high work-hardenability, play an essential role in the strengthening process of austenitic stainless steels. Because of these favorable effects, the HNSS can be a potential material for future structural component application.

Because of the favorable strength, toughness and corrosion resistance, several high strength steels and stainless steels have been used for the fracture and corrosion critical components of carrier-based aircraft. However, some of their properties are not sufficient and remain to be improved. For example, many steel components must have protective coating to prevent corrosion-related damage and premature failure, raising the initial investment and the subsequent life-cycle costs. In order to understand the metallurgical, mechanical, and corrosion characteristics of current and newly emerged steels, to clarify their capability and limitation, and to explore the possibilities of their property improvement, the Airframe Alloy Team of Aerospace Materials Division, Patuxent River has been studying several steels (references 1-20). Some key results of those studies are compiled into this report.

EXPERIMENTAL PROCEDURE

MATERIAL AND HEAT TREATMENT

As the specimen materials, slabs or round rods of high strength steels (4340, 300M, AerMet 100, Hy-Tuf and Ferrium S53) and stainless steels (HNSS, 13-8Mo, Custom 465 and MLX17) were selected. Their nominal chemical compositions are shown in tables B-1 and B-2. These materials were subjected to the following heat treatments, respectively.

- 4340: solution treating at 843^{o}C (1,550^{o}F) for 1 hr, oil-quenching to about 66^{o}C (150^{o}F), tempering at 232^{o}C (450^{o}F) for 3 hr, and air-cooling

- 300M: solution treating at 871^{o}C (1,600^{o}F) for 5 hr in vacuum, oil-quenching to below 71^{o}C (160^{o}F), and double tempering at 301^{o}C (575^{o}F) for 2 hr each in vacuum

- AerMet 100: preheating at 593^{o}C (1,100^{o}F) for 1.25 hr in vacuum, solution treating at 885^{o}C (1,625^{o}F) for 1.25 hr in vacuum, cooling in nitrogen atmosphere, freezing in dry-ice and alcohol (-73^{o}C or –99^{o}F) for 2 hr, and aging at 482^{o}C (900^{o}F) for 5 hr in air

- Hy-Tuf: normalizing at 927^{o}C (1,700^{o}F) for 1 hr, air-cooling, solution treating at 871^{o}C (1,600^{o}F) for 1 hr, oil-quenching, tempering at 260^{o}C (500^{o}F) for 4 hr, and air-cooling

- Ferrium S53: solution treating at 1,050^{o}C (1,922^{o}F) for 70 min, quenching in gas or liquid media such that parts are cooled to 66^{o}C (150^{o}F) within 10 min, freezing in liquid nitrogen within 1 hr of solution treatment for 1 hr followed by air-warming to room temperature, tempering at 482^{o}C (900^{o}F) for 8 hr, quenching or air-cooling to room temperature, freezing in liquid nitrogen within 1 hr of quenching for 1 hr followed by air-warming to room temperature, tempering at 482^{o}C (900^{o}F) for 8 hr, and air-cooling

- HNSS: solution treating at 1,150^{o}C (2,102^{o}F) for 30 min and water-quenching

- 13-8Mo: solution treating at 927°C (1,700°F) for 1.5 hr, water-quenching, aging at 551°C (1,025°F) for 4 hr, and air-cooling

- Custom 465: solution treating at 982°C (1,800°F) for 1 hr, liquid-quenching, freezing to -73°C (-100°F) for 8 hr, warming to room temperature, aging at 538°C (1,000°F) for 4 hr, and air-cooling

- MLX17: solution treating at 840°C (1,545°F) for 2 hr, quenching in oil or water, freezing to -73°C (-100°F) for 8 hr, warming to room temperature, aging at 538°C (1,000°F) for 8 hr, and air-cooling

After the heat treatments, the microstructures of those steels were examined with an optical microscope. The microstructures are shown in figures A-1 and A-2.

SPECIMEN

The slabs and round rods were machined to the following specimens, employing an electrical discharge machine.

- round tension test specimen of gage section diameter 6.4 mm (0.25 in.) in L orientation for tension test (ASTM E 8 – 99)

- hourglass specimen of minimum diameter 6.4 mm (0.25 in.) in L orientation for stress-life fatigue test (ASTM E 466 – 99)

- compact tension specimens, 38.1 mm (1.5 in.) wide and 4.8 mm (3/16 in.) thick, in L-T crack plane orientation for fatigue crack growth (FCG) test (ASTM E 647 – 95a)

- square bar specimens of 10 x 10 x 70 mm (0.4 x 0.4 x 2.8 in.) in L orientation with a Charpy notch at the mid-length for SCC test under four-point bending (ASTM F 1624-95)

TESTS

Tension Test: A closed-loop servo-hydraulic mechanical test machine, Interlaken, of 90 KN (20 kip) capacity was utilized for the tension test. The test was conducted with the tension test specimen in air, following the ASTM E 8 – 01, Standard Test Methods for Tension Testing of Metallic Materials. The tensile loading rate was 0.076 mm/min (0.003 in/min).

Stress-Life Fatigue Test: This test was also carried out in the Interlaken of 90 KN (20 kip) capacity, employing the hourglass specimen, under stress control in tension-tension cycling at stress ratio 0.1 and frequency 10 Hz in air and aqueous 3.5% NaCl solution of pH 7.3. This test followed the ASTM E 466 – 96, Standard Practice for Conducting Force Controlled Constant Amplitude Axial Fatigue Tests of Metallic Materials.

Fatigue Crack Growth Test: Two closed-loop servo-hydraulic mechanical test machines were used for the FCG test. One was a 500 KN (110 kip) vertical Material Testing System machine for the test in vacuum and air, and the other a 45 KN (10 kip) horizontal test machine for the test in liquid. The test was performed under stress control in tension-tension cycling of frequency 10 Hz with a sinusoidal waveform and stress ratios, 0.1 and 0.9, in vacuum of 4×10^{-8} torr, air and aqueous 3.5% NaCl solution of pH 7.3 at room temperature. The fatigue loading procedure was K-decreasing or load shedding with K-gradient parameter C = -0.08 mm^{-1} (-1 $in.^{-1}$) in the near-threshold FCG regime and K-increasing in the Paris and rapid unstable crack growth regimes. Using compliance technique, the fatigue crack length was continuously monitored with a laboratory computer system, interfaced with the test machine. This test followed the ASTM E 647 – 00, Standard Test Method for Measurement of Fatigue Crack Growth Rates.

Open Circuit Potential Measurement: Open circuit potential (OCP) is an electrochemical parameter of corrosion resistance and measurable in a corrosion cell, consisting of a specimen electrode and a reference electrode (saturated calomel electrode [SCE]) in an electrolyte. In this study, the specimen electrode was a rectangular flat sheet of a high strength steel or a stainless steel, 38 x 7 x 1 mm. The specimen surface was coated with Stop-Off Lacquer, except an area of 5 x 7 mm on one face. This area became the working electrode in the electrolyte, aqueous 3.5% NaCl solution of pH 7.3. The specimen and reference electrodes were connected to the ground terminals of an electrometer, and the electrode potential and its change with time were recorded in reference to the SCE. The electrode potential, stabilized after a prolonged exposure period (24 hr), was taken as the OCP.

Stress Corrosion Cracking Test: Since the cantilever bend or double cantilever beam SCC test takes a long time, an accelerated SCC test was conducted in a RSL 1000 SI-Multi-Mode Test System (reference 21). This System included a bending frame, a tensile loading frame, an electrolyte reservoir, a pump for electrolyte circulation, a saturated calomel electrode, a platinum counter-electrode, a PC and a printer. The precracked specimen was step-loaded until the load dropped in four-point bending under constant displacement control, while held at a given potential in aqueous 3.5% NaCl solution of pH 7.3. The load drop at the open circuit potential corresponds to the threshold stress intensity for stress corrosion crack growth, K_{ISCC}.

Fractography: After the fatigue and SCC tests, the fracture surface morphology was examined with a scanning electron microscope, JEOL JSM-6460LV, operated at an accelerating voltage of 20 kV.

RESULTS AND DISCUSSION

MECHANICAL PROPERTIES

The determined mechanical properties of the high strength and stainless steels are shown in tables B-3 and B-4, respectively. 4340, 300M, and AerMet 100 have similar UTS, YS, and hardness. But AerMet 100 has greater fracture toughness K_{IC}, 126 MPa√m (115 ksi√in.), and threshold stress intensity for stress corrosion cracking K_{ISCC}, 25 MPa√m (23 ksi√in.), compared to those for 4340 and 300M. Ferrium has high UTS, 1,986 MPa (288 ksi), and K_{ISCC}, 38 MPa√m (35 ksi√in.), but lower YS, 1,572 MPa (228 ksi). Among the high strength steels, Hy-Tuf has the lowest UTS, YS, and hardness, whereas its K_{IC} and K_{ISCC} are comparatively high. Custom 465 has greater UTS and YS than those for the other stainless steels, HNSS, 13-8Mo and MLX17. All of those stainless steels have quite high K_{ISCC} values, greater than 65 MPa√m (59 ksi√in.) and those for the high strength steels. The fracture toughness is greatest, K_Q = 120 MPa√m (107 ksi√in.), for 13-8Mo, and least, K_Q = 54 MPa√m (49 ksi√in.), for HNSS.

FATIGUE BEHAVIOR

STRESS-LIFE FATIGUE OF HIGH STRENGTH AND STAINLESS STEELS

Stress-life curves are shown for the high strength steels (4340, AerMet 100, Ferrium, and Hy-Tuf) and stainless steels (HNSS, 13-8Mo, Custom 465 and MLX17) in figures A-3 and A-4, respectively. Among the high strength steels, 4340 and Ferrium appear to be slightly more resistant to fatigue fracture than AerMet 100 and Hy-Tuf in air, whereas all four steels have similar susceptibility to corrosion fatigue fracture in 3.5% NaCl solution. Among the stainless steels, 13-8Mo and MLX 17 are more resistant to fatigue fracture than Custom 465 and HNSS in air and than Custom 465 in 3.5% NaCl solution.

FATIGUE CRACK GROWTH IN HIGH STRENGTH STEELS

A schematic curve of FCG rate versus stress intensity range, da/dN versus ΔK, is sketched, indicating the three FCG regimes, in figure A-5. This report follows the Suresh's designation of A for the near-threshold crack growth regime, B for the Paris regime, and C for the rapid unstable crack growth regime (reference 22).

Figure A-6 shows the da/dN versus ΔK curves, indicating the stress ratio effect, for the three high strength steels: 4340, 300M, and AerMet 100. Raising stress ratio, R, from 0.1 to 0.9, shifts the da/dN versus ΔK curve to the left, increasing da/dN and reducing threshold stress intensity range for FCG, ΔK_{th}. In 3.5% NaCl solution, the curve levels off or da/dN is independent of ΔK at R = 0.9 in the B regime.

Figure A-7 shows the environmental effect on FCG in the three high strength steels: 4340, 300M, and AerMet 100. (1) AerMet 100: At R = 0.1, in the A regime, the da/dN is greater in air than in 3.5% NaCl solution and vacuum. In the B regime, the da/dN is still greater in air,

intermediate in 3.5% NaCl solution, and least in vacuum. The lower da/dN in 3.5% NaCl solution than in air is attributable to crack closure induced by corrosion product. In the C regime, the da/dN is similar in air and 3.5% NaCl solution, but it is greater than in vacuum. At R = 0.9, in the A regime, the da/dN is greatest in 3.5% NaCl solution, intermediate in air and smallest in vacuum. This indicates the absence of corrosion-product-induced crack closure at R = 0.9 in 3.5% NaCl solution. In the B regime, the da/dN curve levels off in 3.5% NaCl solution and crosses over the da/dN curve in air and the da/dN is lower in vacuum. In the C regime, the three da/dN versus ΔK curves tends to converge. (2) 300M: At R = 0.1, in the A regime, the da/dN is slightly greater in 3.5% NaCl solution than in air. However, it is similar in the B and C regimes in air and 3.5% NaCl solution. The da/dN is lowest in vacuum in the A and B regimes. The three da/dN versus ΔK curves tend to merge in the C regime. At R = 0.9, the da/dN is greatest in 3.5% NaCl solution, intermediate in air and least in vacuum in the A and B regimes. The da/dN versus ΔK curve in 3.5% NaCl solution levels off in the B regime, and the three curves in the three environments merge in the C regime. (3) 4340: The main features of da/dN variation with ΔK are similar to those for the 300M in the respective environments.

Figure A-8 shows the material effect on FCG in the three environments. (1) Vacuum: At R = 0.1, in the A regime, da/dN is greatest for 300M, intermediate for AerMet 100, and least for 4340. In the B regime, da/dN is greatest for 300M and AerMet 100, and lowest for 4340. In the C regime, the three curves tend to merge. This indicates that 4340 is more resistant to FCG than AerMet 100 and 300M at R = 0.1 in the absence of corrosive environment. At R = 0.9, in the A regime, the three da/dN versus ΔK curves overlap each other. In the B and C regimes, the da/dN is similar for 300M and 4340, whereas that of AerMet 100 is least. (2) Air: At R = 0.1, in the A regime, da/dN is greatest for Ferrium, slightly less for 4340, intermediate for 300M and least for AerMet 100. However, in the B and C regimes, the four da/dN versus ΔK curves overlap each other, indicating similar da/dN. At R = 0.9, in the A regime, the three da/dN versus ΔK curves nearly overlap each other. In the B and C regimes, the da/dN versus ΔK curves of 300M and 4340 nearly overlap each other, and da/dN is lowest for AerMet 100. (3) 3.5% NaCl solution: At R = 0.1, throughout the three regimes, da/dN is greater for Ferrium and 4340, intermediate for 300M, and least for AerMet 100. This observation evidences that the resistance to corrosion FCG is greatest for AerMet 100, intermediate for 300M and least for Ferrium and 4340 at R = 0.1 in 3.5% NaCl solution. At R = 0.9, the four da/dN versus ΔK curves level off, and the level is highest for 4340, intermediate for 300M, and lowest for Ferrium and AerMet 100.

During corrosion fatigue test of Ferrium specimens in 3.5% NaCl solution, red rust was observed coming from the crack surface, as shown in figure A-9. This confirms that Ferrium is not stainless, as expected from its not-high Cr-concentration, 9.4%.

VARIATION OF FATIGUE CRACK GROWTH/TIME, da/dt, WITH MAXIMUM STRESS INTENSITY, K_{max}, IN HIGH STRENGTH STEELS

For the fatigue test in 3.5% NaCl solution, the FCG per cycle, da/dN, is converted to the corresponding crack growth per unit time, da/dt, following the relationship da/dt = f(da/dN), where f is the loading frequency. The da/dt is plotted against the maximum stress intensity, K_{max}.

Also, the SCC growth rate, da/dt, in 3.5% NaCl solution is plotted against the applied stress intensity, K_I (references 17 and 23). The plots for the three high strength steels are shown in figure A-10. The upper portion of the da/dt versus K_{max} curve is in the region of $K_{max} > K_{ISCC}$, more at R = 0.9 than at R = 0.1. Furthermore, the da/dt versus K_{max} curve for FCG at R = 0.9 and the da/dt versus K_I curve for stress corrosion crack growth are closely located and their shapes are somewhat similar. In the region of the $K_{max} > K_{ISCC}$, SCC appears to take place during fatigue loading, especially at higher da/dN and more at R = 0.9.

FATIGUE CRACK GROWTH IN STAINLESS STEELS

Figure A-11 shows the da/dN versus ΔK curves, indicating the stress ratio effect, for the four stainless steels: HNSS, 13-8Mo, Custom 465, and MLX17. As for the high strength steels, raising stress ratio, R, from 0.1 to 0.9, shifts the da/dN versus ΔK curve to the left, increasing the da/dN and reducing the ΔK_{th}. At R = 0.9 in 3.5% NaCl solution, the curve levels off or da/dN is independent of ΔK in the B regime. The stress ratio effect is more obvious for the Custom 465 in 3.5% NaCl solution, showing greater separation and shape difference in the da/dN versus ΔK curve at R = 0.1 and 0.9.

Figure A-12 indicates the environmental effect on the da/dN variation with ΔK for the four stainless steels. (1) HNSS: At R = 0.1 and 0.9 in the A and B regimes, ΔK_{th} is less and da/dN is greater in 3.5% NaCl solution than in air. In the C regime, the da/dN versus ΔK curves tend to merge in the both environments. (2) 13-8Mo: The da/dN versus ΔK curves nearly overlap at R = 0.1 and 0.9 in air and 3.5% NaCl solution, except smaller ΔK_{th} and greater da/dN at R = 0.9 in 3.5% NaCl solution than in air for the A regime. (3) Custom 465: At R = 0.1, the da/dN versus ΔK curves nearly overlap in air and 3.5% NaCl solution. However, at R = 0.9, the ΔK_{th} is much less in 3.5% NaCl solution than in air, and the da/dN versus ΔK curve in 3.5% NaCl solution levels off in the B regime. (4) MLX 17: At R = 0.1 and 0.9, the ΔK_{th} is less in 3.5% NaCl solution than in air, the da/dN versus ΔK curve levels off in the B regime in 3.5% NaCl solution, and the da/dN versus ΔK curves in the both environments tend to merge in the C regime.

Figure A-13 shows the material effect on FCG in air and 3.5% NaCl solution for the four stainless steels. In air, the da/dN versus ΔK curves for 13-8Mo and Custom 465 nearly overlap at R = 0.1, those for 13-8Mo, Custom 465 and MLX17 overlap at R = 0.9, and the ΔK_{th} is greatest and da/dN is least in the A regime for the HNSS. In 3.5% NaCl solution, the da/dN versus ΔK curves for the four stainless steels overlap totally or partly at R = 0.1. The da/dN versus ΔK curve of Custom 465 stainless steel is separated from the other three nearly overlapping curves, having the lowest ΔK_{th} at R = 0.9.

FRACTOGRAPHIC FEATURES

HIGH STRENGTH STEELS

In vacuum and air, at R = 0.1, the fractographic features are relatively similar for the three high strength steels, 4340, 300M and AerMet 100; cleavage facets at lower da/dN and enlarged cleavage facets and dimples at higher da/dN. At R = 0.9, the number and size of dimple increase more with increasing da/dN, figures A-14 and A-15. This observation evidences that, in vacuum and air, the cleavage facet is enlarged, the number and size of dimple increase, and the enlarged cleavage facets are disintegrated and replaced by dimples more with increasing da/dN and R (reference 17).

In 3.5% NaCl solution, at R = 0.1, cleavage facets and some dimples are seen at lower da/dN (or da/dt) and enlarged cleavage facets at higher da/dN for the AerMet 100. However, at R = 0.9, mixed cleavage and intergranular facets are visible at lower da/dN and mostly dimples at higher da/dN for the AerMet 100. More intergranular facets are present at higher da/dN and R = 0.1, and mixed cleavage and intergranular facets at lower da/dN and mostly intergranular facets at higher da/dN for the 300M (reference 17). On the other hand, mostly intergranular facets are present at low and high da/dN and R = 0.1 and 0.9 for the 4340, figure A-16. This observation evidences that, in 3.5% NaCl solution:

- Cleavage facets and dimples are seen at lower R and da/dN in more corrosion fatigue resistant steel, such as the AerMet 100. However, these fractographic features are replaced by mixed cleavage and intergranular facets at higher R and lower da/dN, and they are mostly replaced by dimples at higher da/dN.

- In lower corrosion fatigue resistance steels, such as the 300M and 4340, more intergranular facets cover the crack surface at low and high da/dN and R (reference 17).

At the beginning of SCC in 3.5% NaCl solution, the fractographic features are predominantly intergranular facets for the three steels. At the later stage of SCC, intergranular facets, secondary cracks, and dimples are visible.

These observations indicate that the susceptibility to intergranular cracking or grain boundary decohesion is greatest for the 4340, somewhat less for the 300M, and least for the AerMet 100 during fatigue and SCC in 3.5% NaCl solution. Considering the K_{ISCC} values of the three steels, the least for 4340, slightly greater for 300M, and the greatest for AerMet 100, the greater susceptibility to intergranular cracking corresponds to the smaller K_{ISCC} or the smaller SCC resistance.

The scanning electron microscopy (SEM) fractographs of Ferrium, fatigued in air, show striation-bands in the regime of lower da/dN or regime A, striations of greater spacing and small patches of dimples in the regime B, and disintegrated striations and more dimples in the regime C, figure A-17a, b, and c. Those, fatigued in 3.5% NaCl solution, show corrosion products with

mud-cracks covering the fracture surface, figure A-17d, e, and f, indicating the high susceptibility of Ferrium to corrosion in 3.5% NaCl solution.

STAINLESS STEELS

The SEM fractographs of 13-8Mo, fatigued in air, show striation patches covering the fracture surface in the regime A, striation patches and small number of dimple in the regime B, and few striation patches and larger dimples in the regime C, figure A-18a, b, and c. Those, fatigued in 3.5% NaCl solution, show a few cleavage facets and a small number of dimples in the regime A, mostly striations of enlarged spacing in the regime B, and a decreasing number of striation of enlarged spacing and more dimples in regime C, figure A-18d, e, and f.

The SEM fractographs of Custom 465, fatigued in air, show striation patches and cleavage facets in the regime A, and patches of striation of enlarged spacing and a small number of dimples in the regimes B and C, figure A-19a, b, and c. Those, fatigued in 3.5% NaCl solution, show a mixture of cleavage and intergranular facets and secondary cracks along grain boundaries in the regime A, intergranular facets with corrosion pits and secondary cracks along grain boundaries in the regime B and C, figure A-19d, e and f. More corrosion pits are noticeable on the intergranular facets in the regime C.

The SEM fractographs of MLX17, fatigued in air, show cleavage facets and striation patches in the regime A, decreasing number of cleavage facets and striation patches, and some dimples in the regime B, and few cleavage facets, more dimples, and no visible striation in the regime C, figure A-20a, b, and c. Those, fatigued in 3.5% NaCl solution, show a few patches of cleavage facets in the regime A, striations and cleavage facets in the regime B, and few cleavage facets, more dimples and no visible striations in the regime C, figureA-18d, e, and f.

CONCLUSIONS

AerMet 100 is the best available high strength and high toughness steel, but it requires better corrosion resistance.

The four stainless steels (HNSS, 13-8Mo, Custom 465, and MLX 17) have good corrosion resistance, but they require greater strength and toughness for fracture critical components.

RECOMMENDATIONS

The following is recommended:

- Development of a stainless steel of
  - YS $\geq$ 250 ksi
  - UTS $\geq$ 285 ksi
  - $K_{IC} \geq 100$ ksi$\sqrt{\text{in.}}$
  - $K_{ISCC} \geq 50$ ksi$\sqrt{\text{in.}}$

- Study on cold-work effect of HNSS and Custom 465 stainless steels, and its improvement (Reportedly, HNSS and Custom 465 stainless steels have good cold-work effect.)

REFERENCES

1. NADC Report No. NADC-91111-60, Fatigue Crack Growth in AerMet 100 Steel, of 18 Oct 1991.

2. NAWCAD Warminster Report No. NAWCADWAR-94001-60, Corrosion Behavior of Landing Gear Steels, of 29 Oct 1993.

3. C. E. Neu, E. U. Lee, E. W. Lee, J. B. Boodey, J. Kozol, J. W. Morris, and J. Waldman, "Characterization of AerMet 100 Steel for Navy Aircraft Applications," Metallic Materials for Lightweight Applications, Edited by M. G. H. Wells, E. B. Kula and J. H. Beaty, (Proceedings of the 40th Sagamore Army Materials Research Conference, 30 Aug - 2 Sep 1993, Plymouth, MA), pp. 389-413.

4. P. F. Buckley, R. Brown, J. H. Graves, E. U. Lee, C. E. Neu, and J. Kozol, “Corrosion Behavior of AerMet 100 Steel," Metallic Materials for Lightweight Applications, Edited by M. G. H. Wells, E. B. Kula, and J. H. Beaty, (Proceedings of the 40th Sagamore Army Materials Research Conference, 30 Aug - 2 Sep 1993, Plymouth, MA), pp. 449-464.

5. Eun U. Lee and Jeffrey Waldman, "Corrosion of Aircraft Landing Gear Steels," Naval Engineers Journal, Nov 1994, pp. 77- 83.

6. E. U. Lee, J. Kozol, J. B. Boody, and J. Waldman, "Corrosion of Landing Gear Steels," AGARD Conference Proceedings 565, Corrosion Detection and Management of Advanced Airframe Materials, (Papers Presented at the 79th Meeting of the AGARD Structures and Materials Panel, Serville, Spain, 5-6 Oct 1994), Jan 1995, AGARD, pp. (4-10) – (4-12).

7. E. U. Lee, "SCC Path in Forged AerMet 100 Steel," Metallurgical and Materials Transactions”, of May 1995.

8. NAWCAD Patuxent River Technical Report No. NAWCADPAX--96-209-TR, Corrosion Fatigue of AerMet 100 Steel, of 9 Jul 1996.

9. NAWCAD Patuxent River Technical Report No. NAWCADPAX--96-126-TR, Surface Treatment Effect on AerMet 100 Steel: Part 1. Shot Peening Effect on Corrosion and Fatigue of AerMet 100 Steel, of 12 Apr 1996.

10. NAWCAD Patuxent River Technical Report No. NAWCADPAX--96-250-TR, Load Ratio Dependence of Fatigue Threshold in AerMet 100 Steel, of 2 Oct 1996.

11. Eun U. Lee, Kenneth George and William E. Frazier, "Environment Assisted Fatigue Cracking of AerMet 100 Steel," Proceedings of 1997 Tri-Service Conference on Corrosion, 17-21 Nov 1997, Wrightsville Beach, NC, Vol. 1, Session 5.

12. NAWCAD Patuxent River Technical Report No. NAWCADPAX--98-109-TR, Notch Sensitivity Effect on Fatigue of AerMet 100 Steel in Air and Salt Air, of 3 Aug 1998.

13. Eun U. Lee, Henry Sanders, and Bhaskar Sarkar, "Stress Corrosion Cracking of High Strength Steels," Proceedings of 1999 Tri-Service Conference on Corrosion, 15-19 Nov 1999, Myrtle Beach, SC.

14. Eun U. Lee, "Stress Corrosion Cracking of HVOF Coated and Cr Plated AerMet 100," HCAT (Hard Chrome Alternatives Team) Report, Mar 2002.

15. E. U. Lee, H. C. Sanders, and S. Hartle, "SCC and Corrosion Fatigue of HVOF Coated and Cr Plated AerMet 100 Steel," Proceedings of 2002 Tri-Service Corrosion Conference, 14-18 Jan 2002, San Antonio, TX, pp. 260 – 277.

16. NAWCAD Patuxent River Technical Report No. NAWCADPAX/TR-2002/243, Corrosion Preventive Compounds for Corrosion Prevention/Mitigation (AerMet 100 Steel), of 29 Jan 2003.

17. NAWCAD Patuxent River Technical Report No. NAWCADPAX/TR-2004/12, Evolution of Fractograph during Fatigue and Stress Corrosion Cracking, of 23 Feb 2004.

18. E. U. Lee and A. K. Vasudevan, "Environmentally Influenced Fatigue in High Strength Steels," in Fatigue and Fracture Mechanics: 34th Volume, ASTM STP 1461, Edited by Steven R. Daniewics, James C. Newman, and Karl-Heinz Schwalbe, Sep 2005, pp. 151-163.

19. NAWCAD Patuxent River Technical Report No. NAWCADPAX/TR-2005/20, Study on Cadmium Replacement for Hy-Tuf Steel, of 9 Mar 2005.

20. Eun U. Lee, Amy Hilgeman, Erin Beck, Steve Brown, and Craig Matzdorf, "Cadmium Alternative Coating Corrosion Performance on 4340 Steel," Proceedings of 2007 Tri-Service Corrosion Conference, 3-7 Dec 2007, Denver, CO, P1792.

21. "The Rising Step-Load Test," ASM Handbook, Vol. 8, Mechanical Testing, ASM International, Jun 1995, pp. 539-40.

22. S. Suresh, "Fatigue of Materials," Cambridge University Press, Cambridge, UK, 1991, p. 203 and 211.

23. A. Oehlert and A. Atrens, "Stress Corrosion Crack Propagation in AerMet 100," Journal of Materials Science, Vol. 33, 1998, pp. 775-781.

APPENDIX A
FIGURES

Figure No.	Title
A-1	Micrographs of High Strength Steels
A-2	Micrographs of Stainless Steels
A-3	Stress-Life Curves for High Strength Steels
A-4	Stress-Life Curves for Stainless Steels
A-5	Schematic Curve of da/dN versus ΔK, showing Three Regimes of Fatigue Crack Growth
A-6	Curves of da/dN versus ΔK, Indicating Stress Ratio Effect
A-7	Curves of da/dN versus ΔK, Indicating Environmental Effect
A-8	Curves of da/dN versus ΔK, Indicating Material Effect
A-9	Ferrium Specimen, Fatigue-Tested in 3.5% NaCl Solution
A-10	da/dt versus K_{max} or K_I Curve for AerMet 100, 300M and 4340 Steels
A-11	da/dN versus ΔK Curves, Indicating Stress Ratio Effect, for Stainless Steels
A-12	da/dN versus ΔK Curves, Indicating Environmental Effect, for Stainless Steels
A-13	da/dN versus ΔK Curves, Indicating Material Effect, for Stainless Steels
A-14	da/dN versus ΔK Curves and SEM Fractographs of 300M Steel, Fatigued in Vacuum
A-15	da/dN versus ΔK Curves and SEM Fractographs of AerMet 100 Steel, Fatigued in Air
A-16	da/dN versus K_{max} and K_I Curves and SEM Fractographs of 4340 Steel, Fatigued in 3.5% NaCl Solution
A-17	SEM Fractographs of Ferrium, Fatigued in Air and 3.5% NaCl Solution
A-18	SEM Fractographs of 13-8Mo, Fatigued in Air and 3.5% NaCl Solution
A-19	SEM Fractographs of Custom 465, Fatigued in Air and 3.5% NaCl Solution 3
A-20	SEM Fractographs of MLX17, Fatigued in Air and 3.5% NaCl Solution

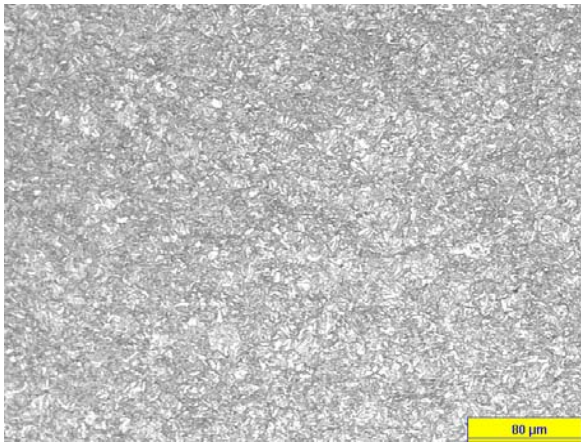

AerMet 100 Steel

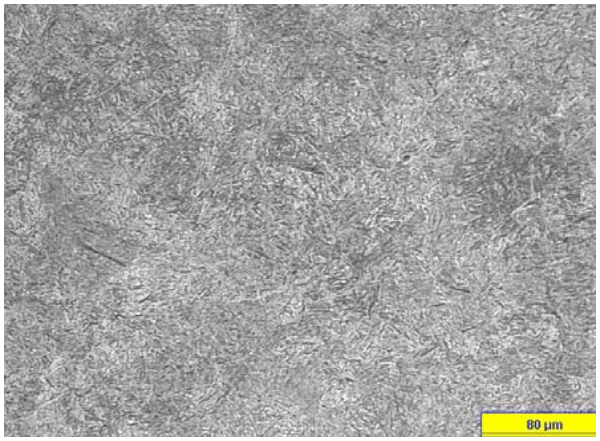

300M Steel

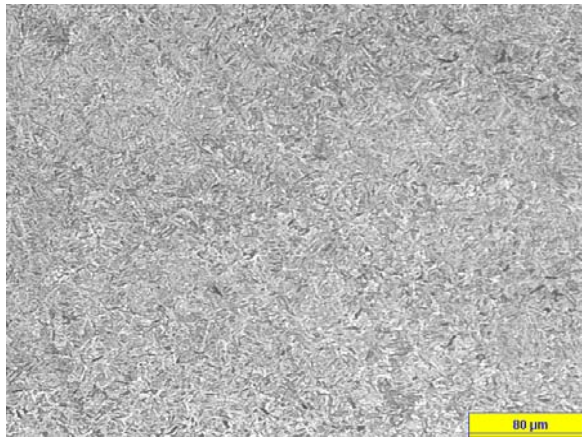

4340 Steel

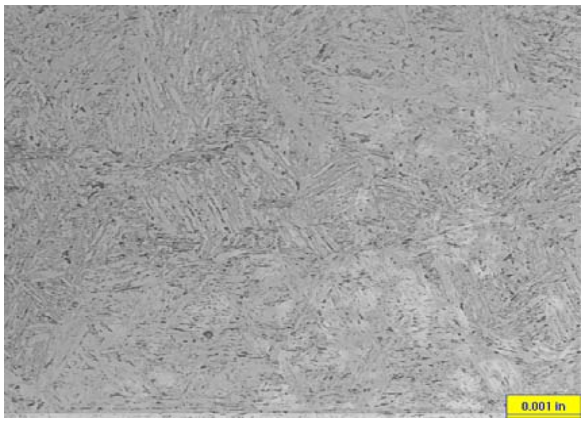

Ferrium

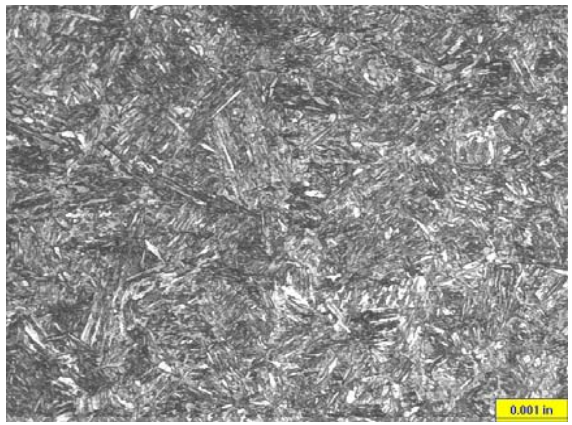

Hy-Tuf

Figure A-1: Micrographs of High Strength Steels

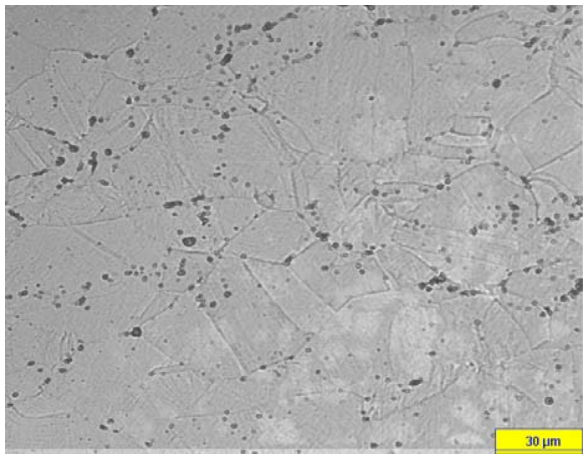

HNSS

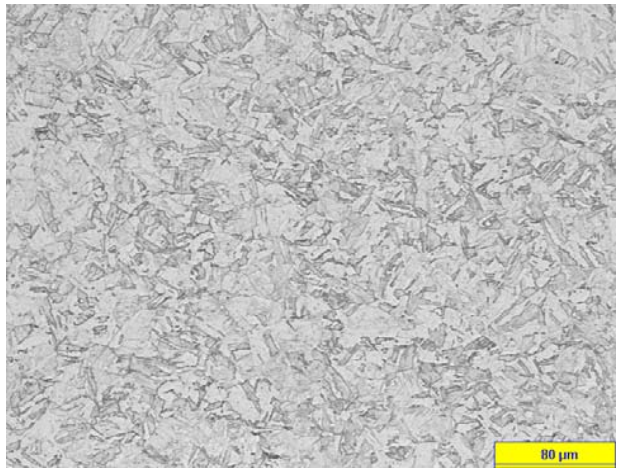

13-8Mo

465

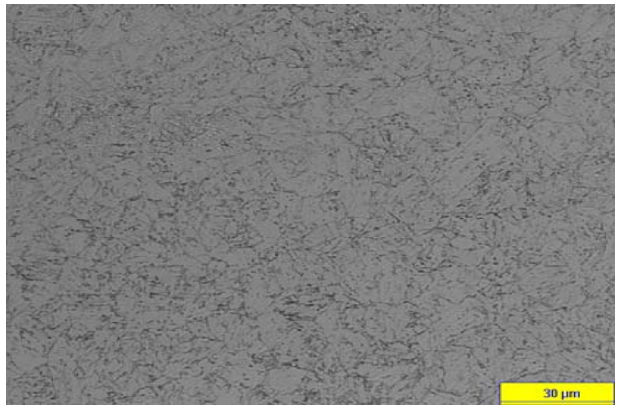

MLX17

Figure A-2: Micrographs of Stainless Steels

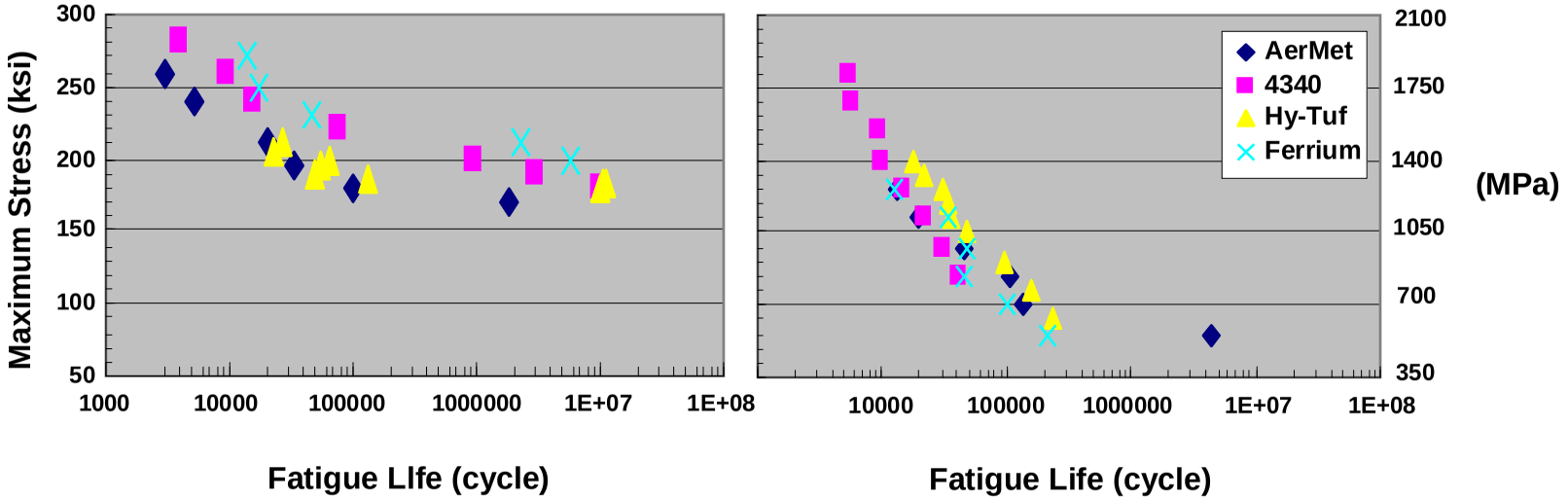

Figure A-3: Stress-Life Curves for High Strength Steels

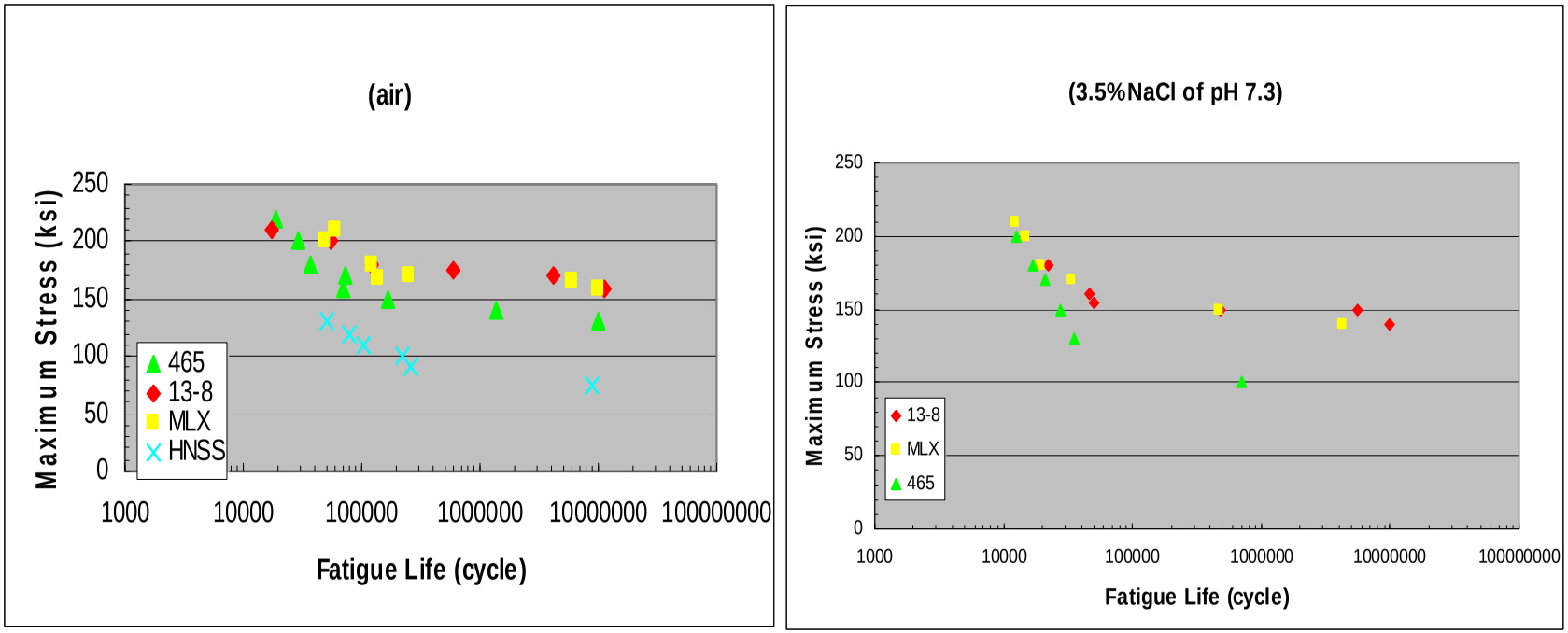

Figure A-4: Stress-Life Curves for Stainless Steels

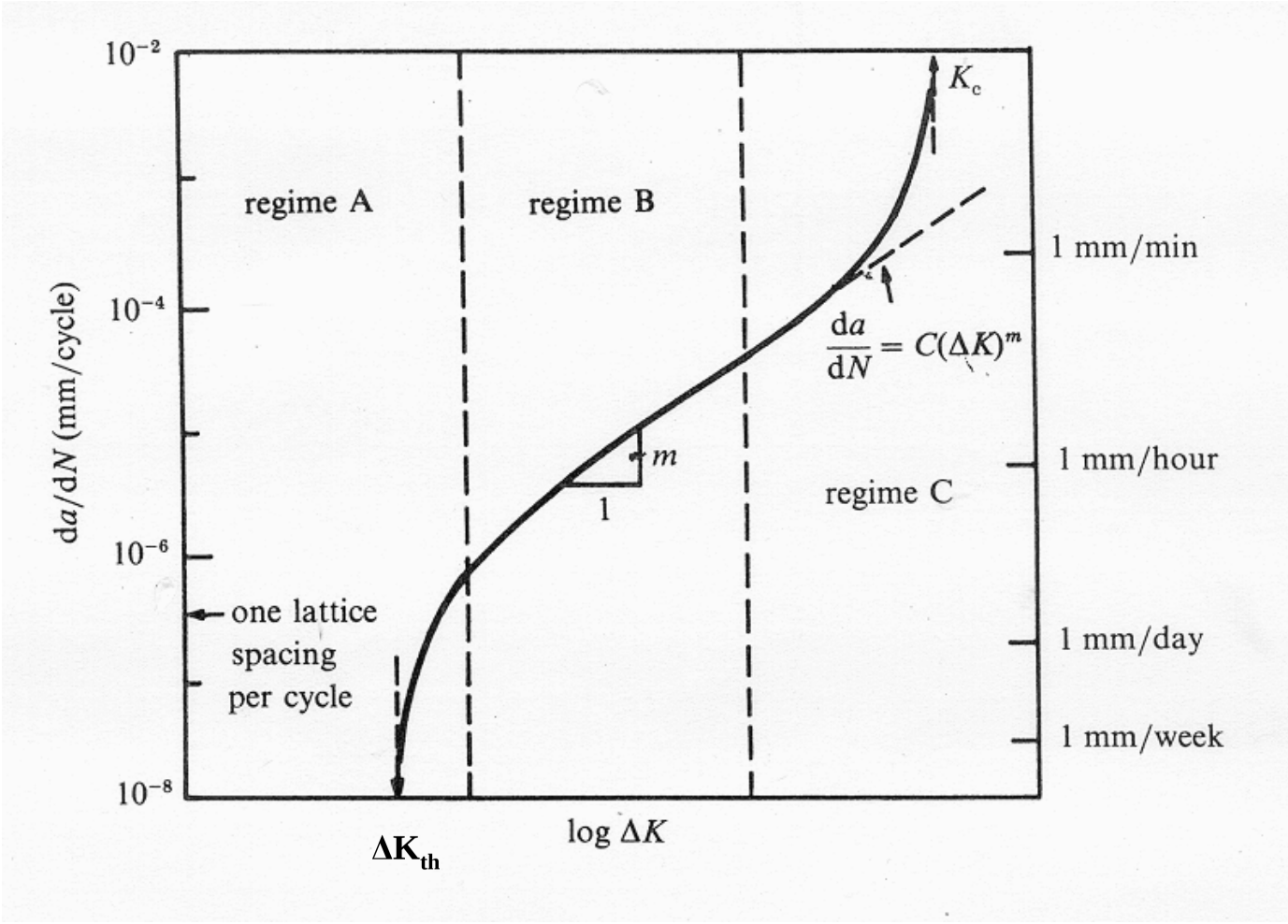

Figure A-5: Schematic Curve of da/dN versus K, Showing Three Regimes of Fatigue Crack Growth

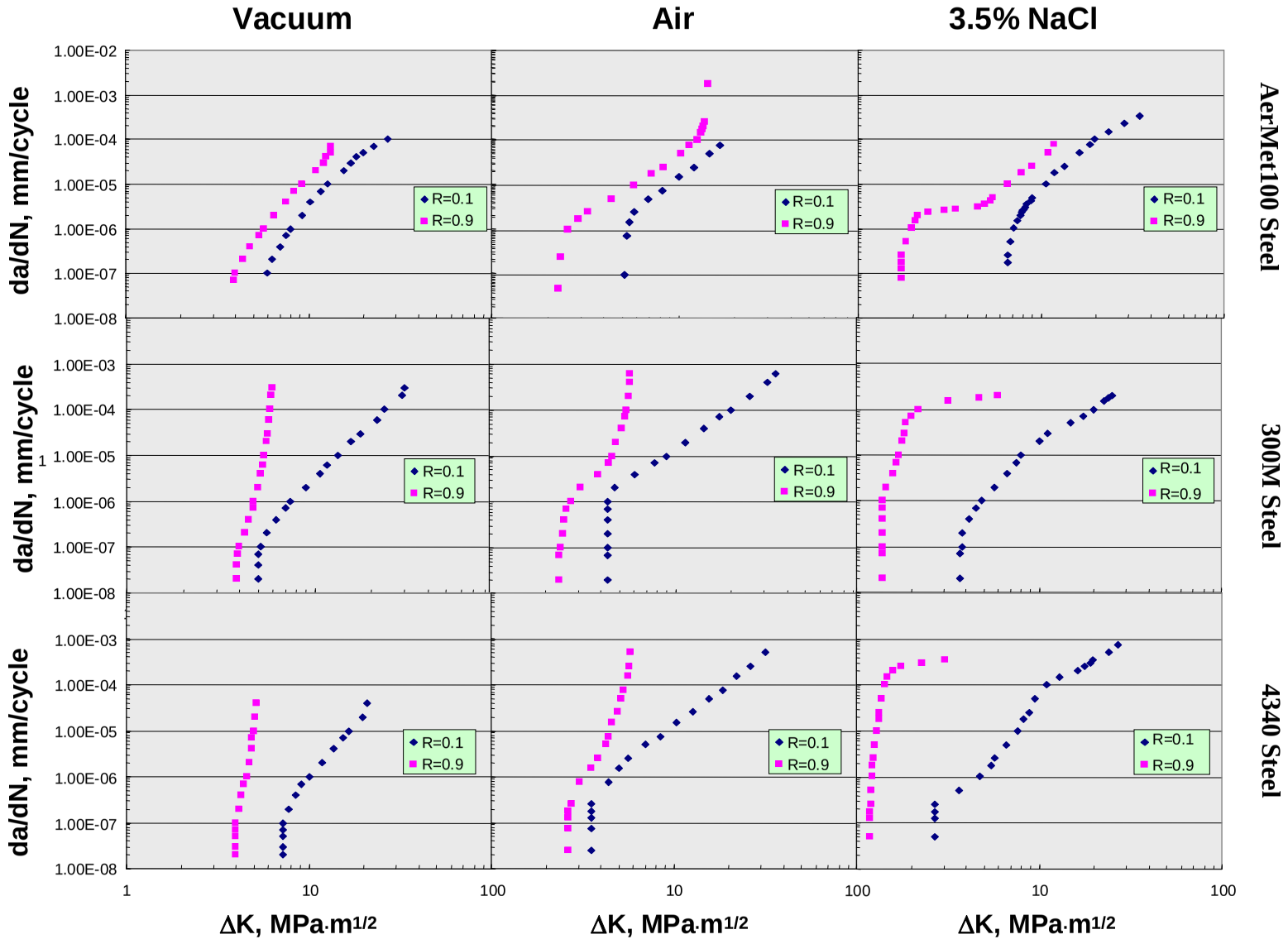

Figure A-6: Curves of da/dN versus ΔK, Indicating Stress Ratio Effect

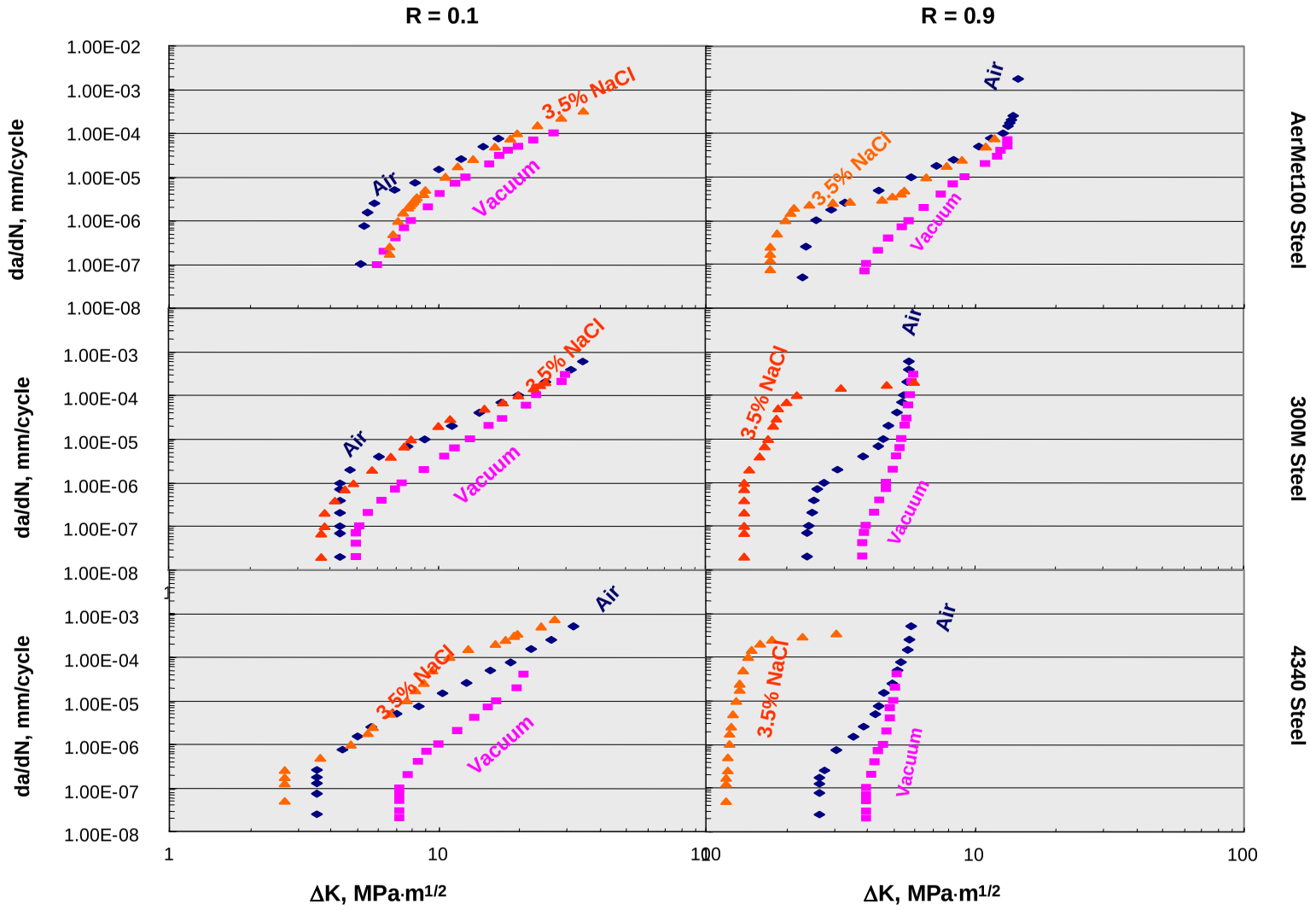

Figure A-7: Curves of da/dN versus K, Indicating Environmental Effect

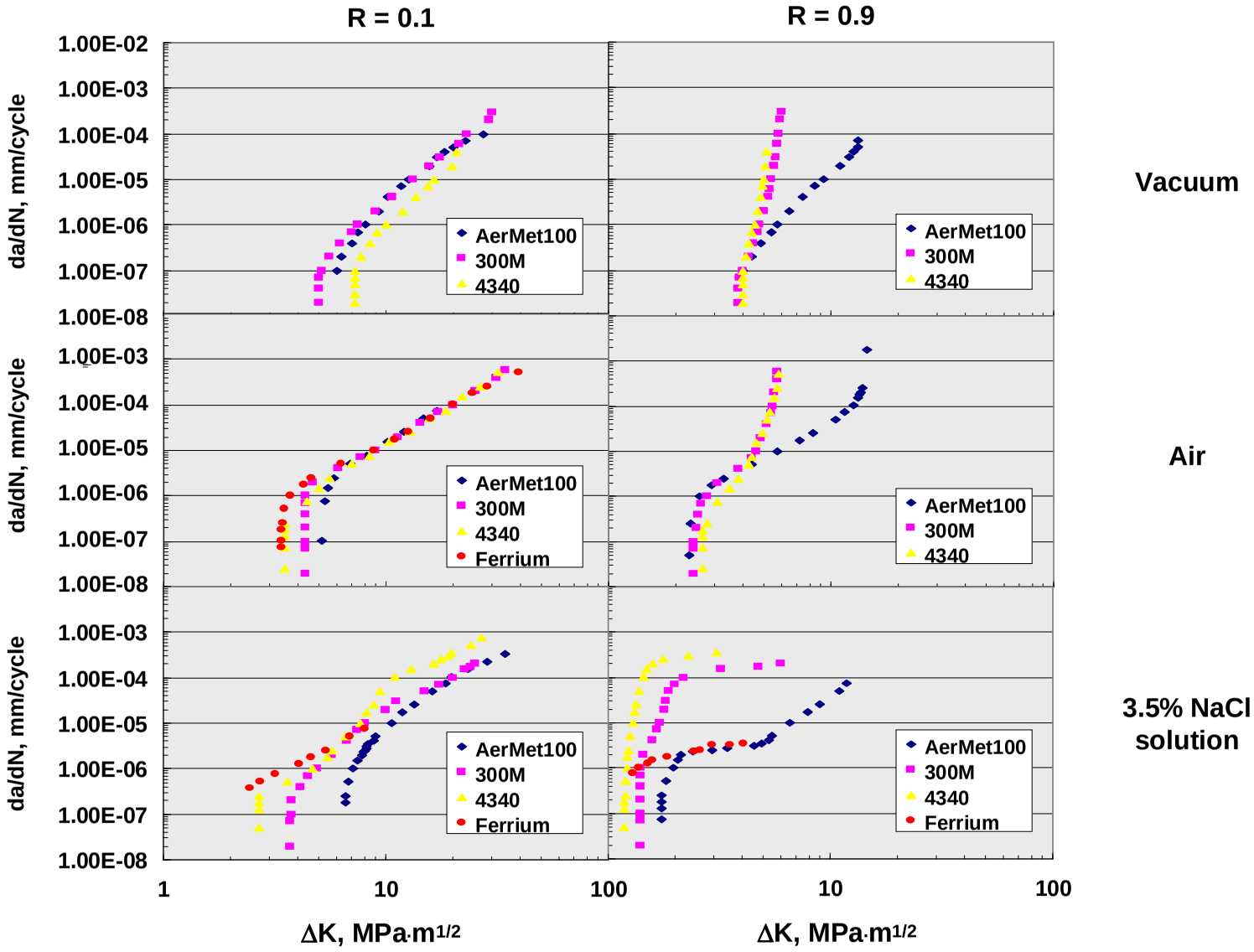

Figure A-8: Curves of da/dN versus K, Indicating Material Effect

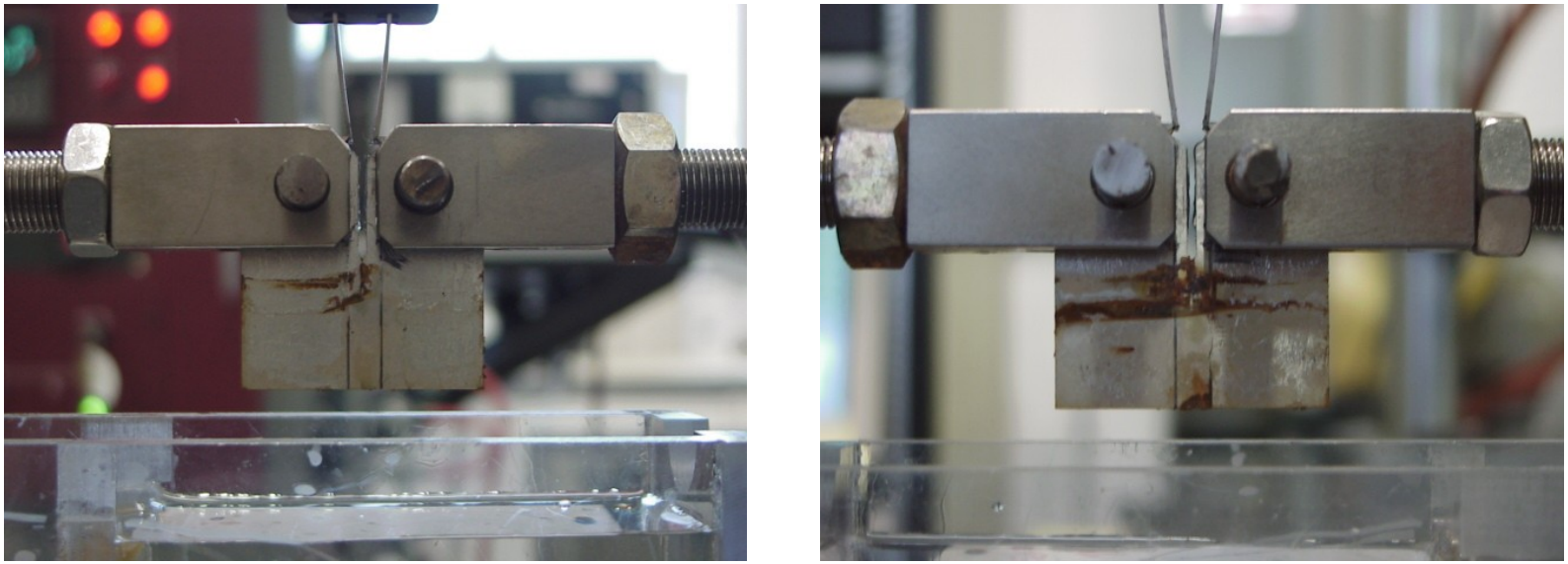

Figure A-9: Ferrium Specimen, Fatigue-Tested in 3.5% NaCl Solution

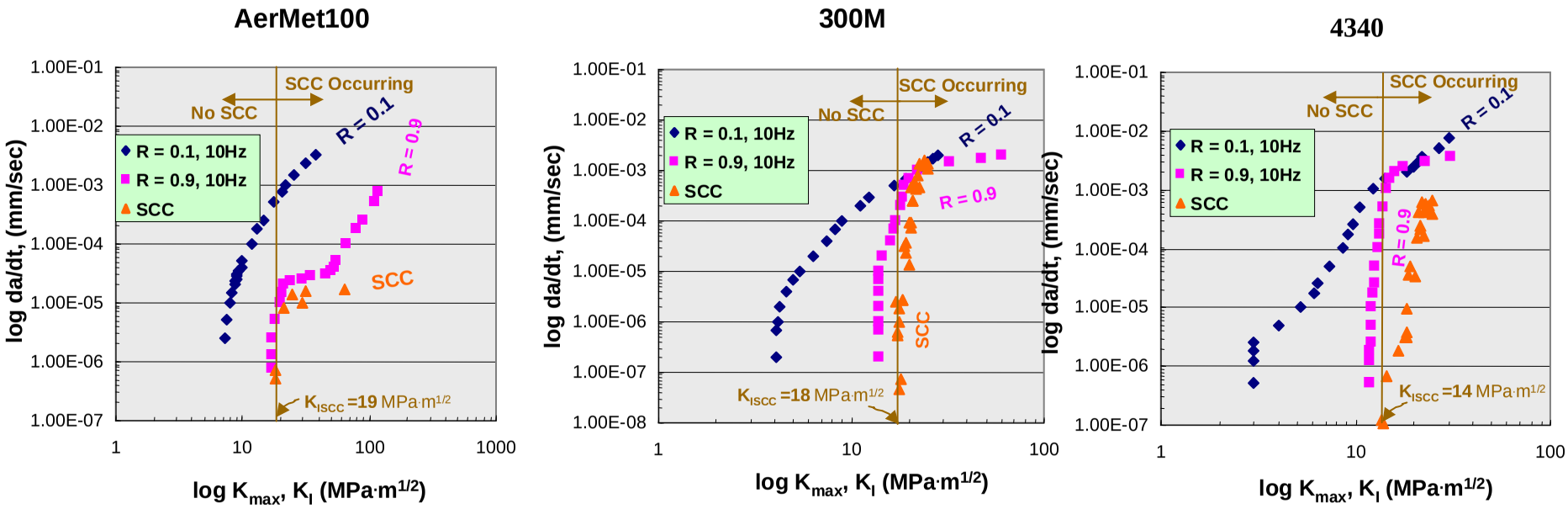

Figure A-10: da/dt versus K_{max} or K_I Curve for AerMet 100, 300M, and 4340 Steels

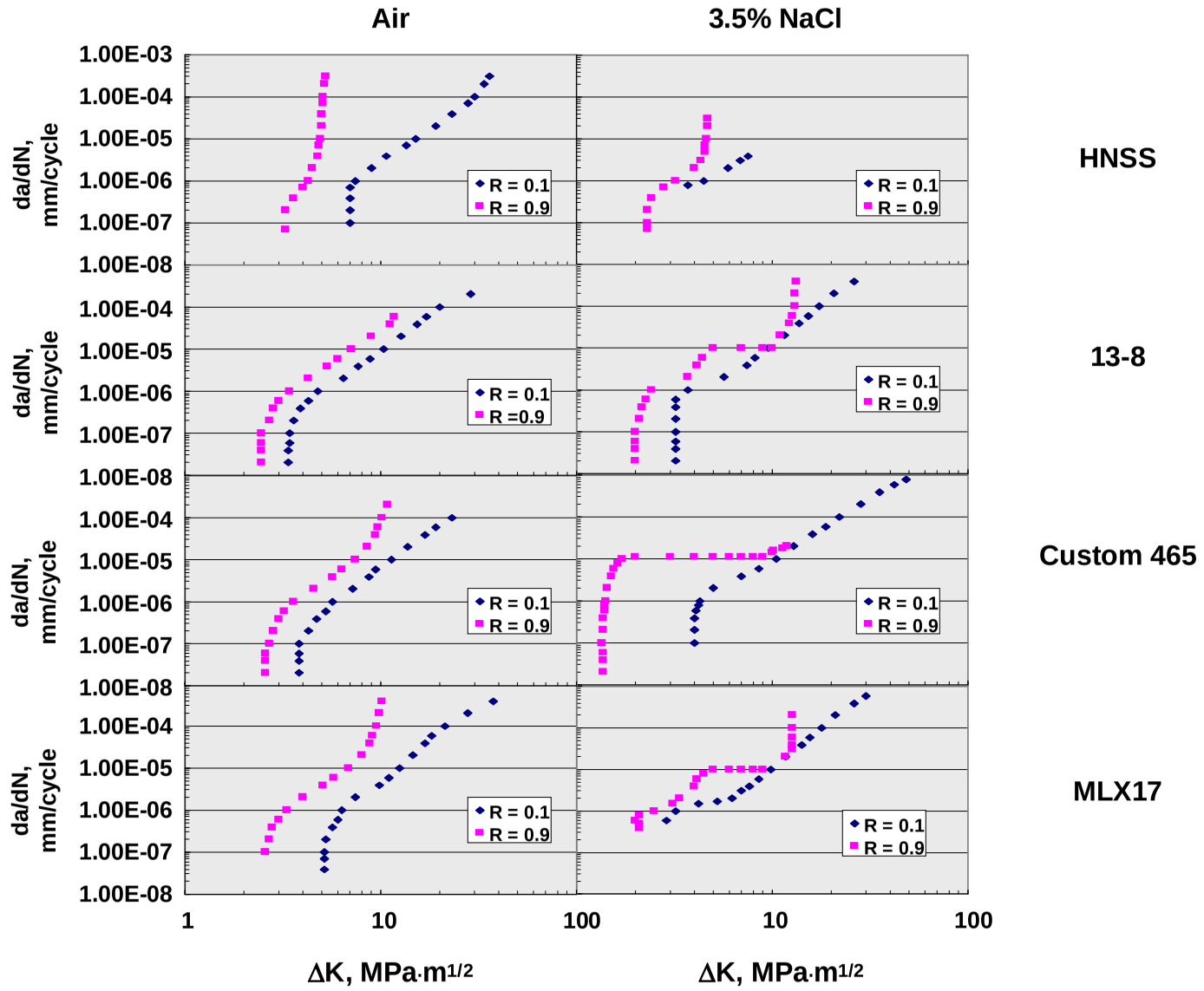

Figure A-11: da/dN versus ΔK Curves, Indicating Stress Ratio Effect, for Stainless Steels

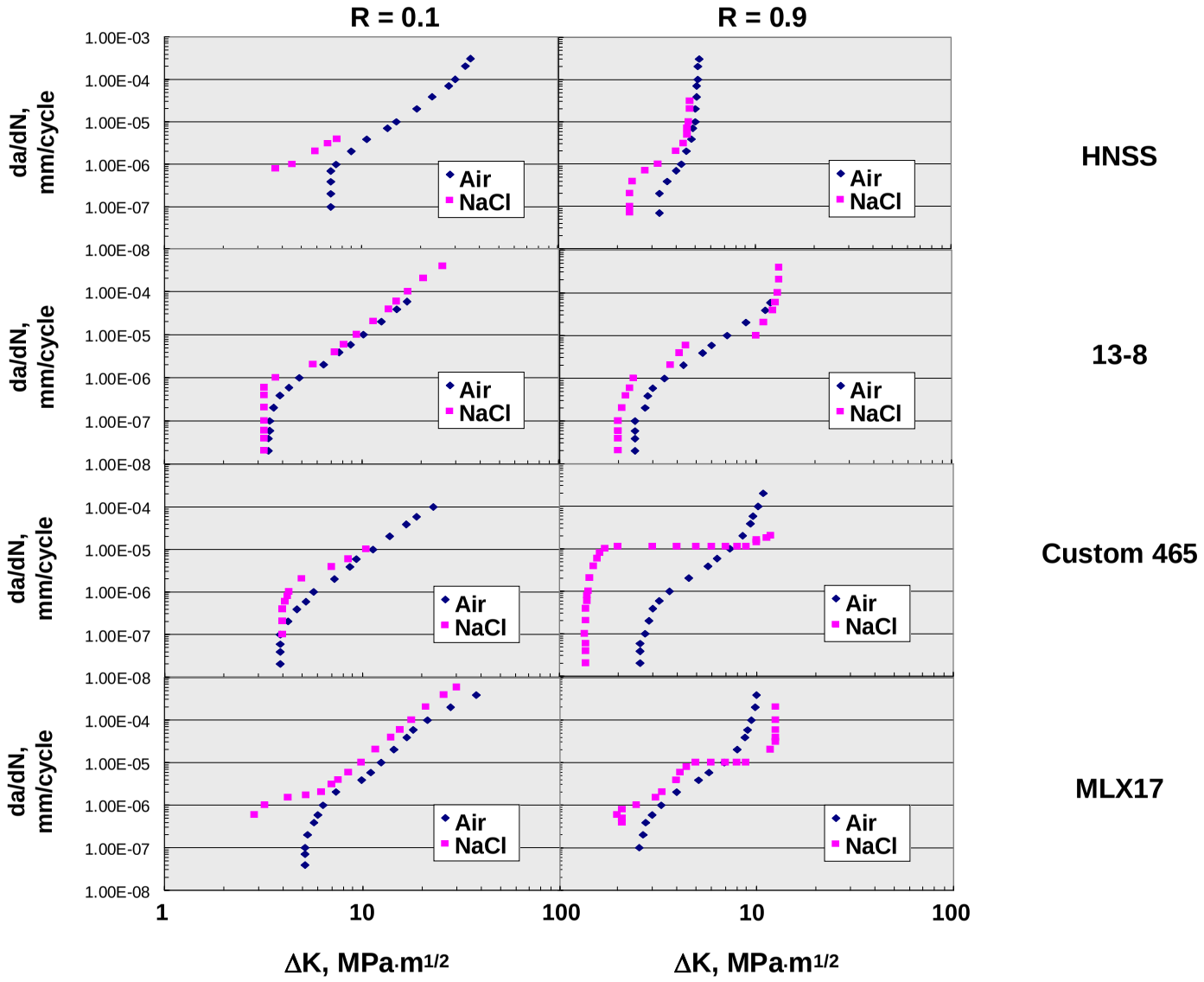

Figure A-12: da/dN versus ΔK Curves, Indicating Environmental Effect, for Stainless Steels

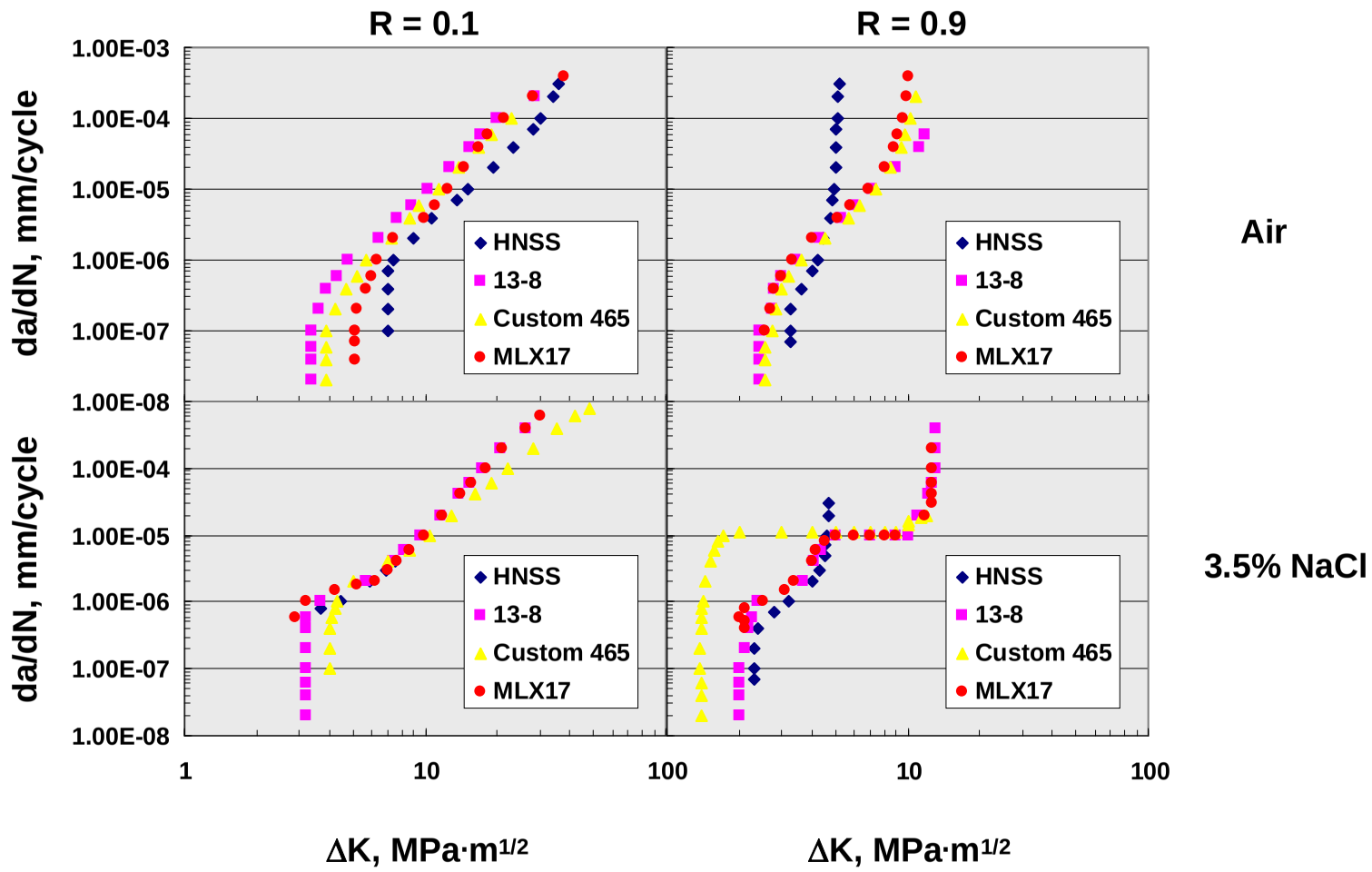

Figure A-13: da/dN versus K Curves, Indicating Material Effect, for Stainless Steels

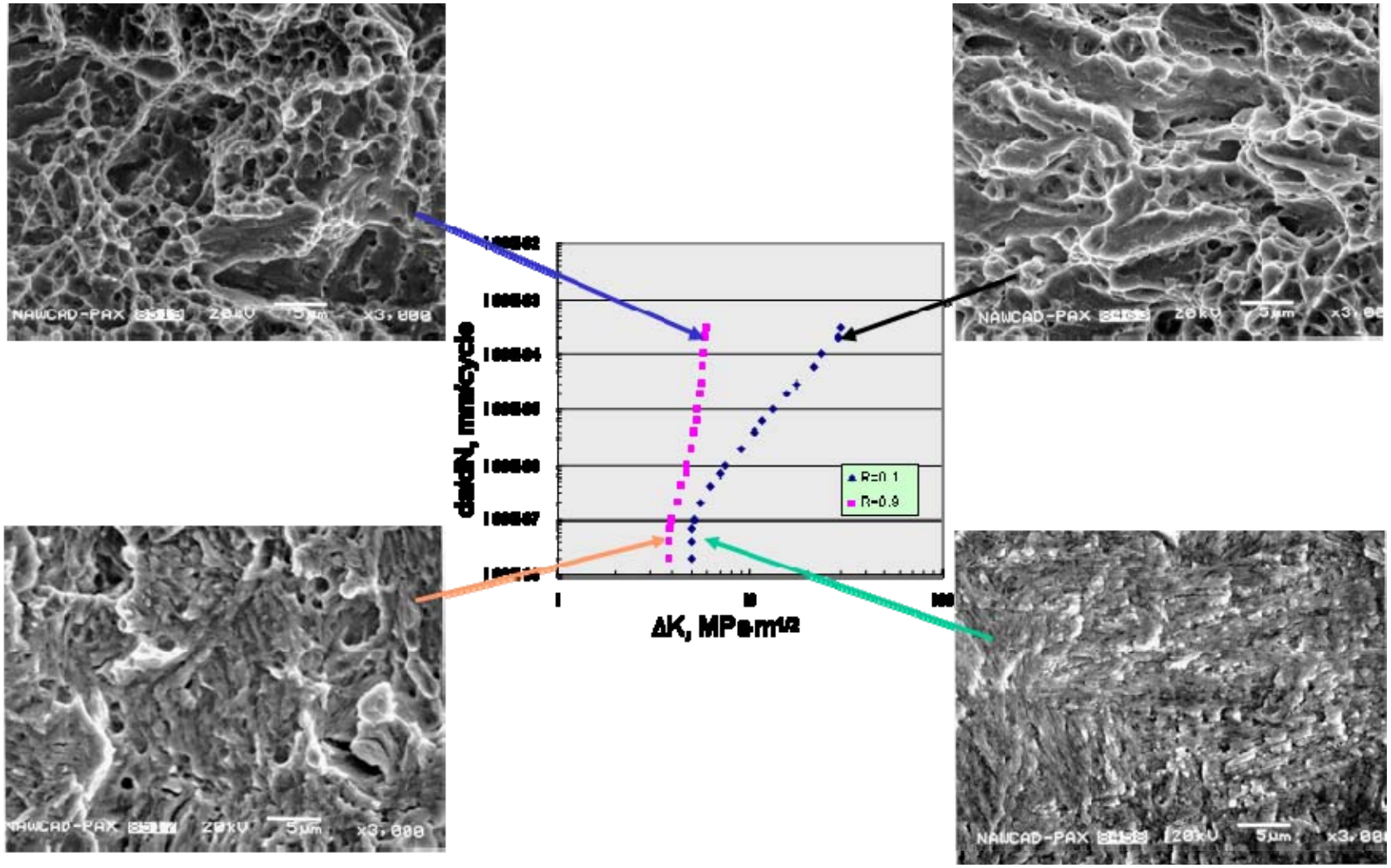

Figure A-14: da/dN versus ΔK Curves and SEM Fractographs of 300M Steel, Fatigued in Vacuum

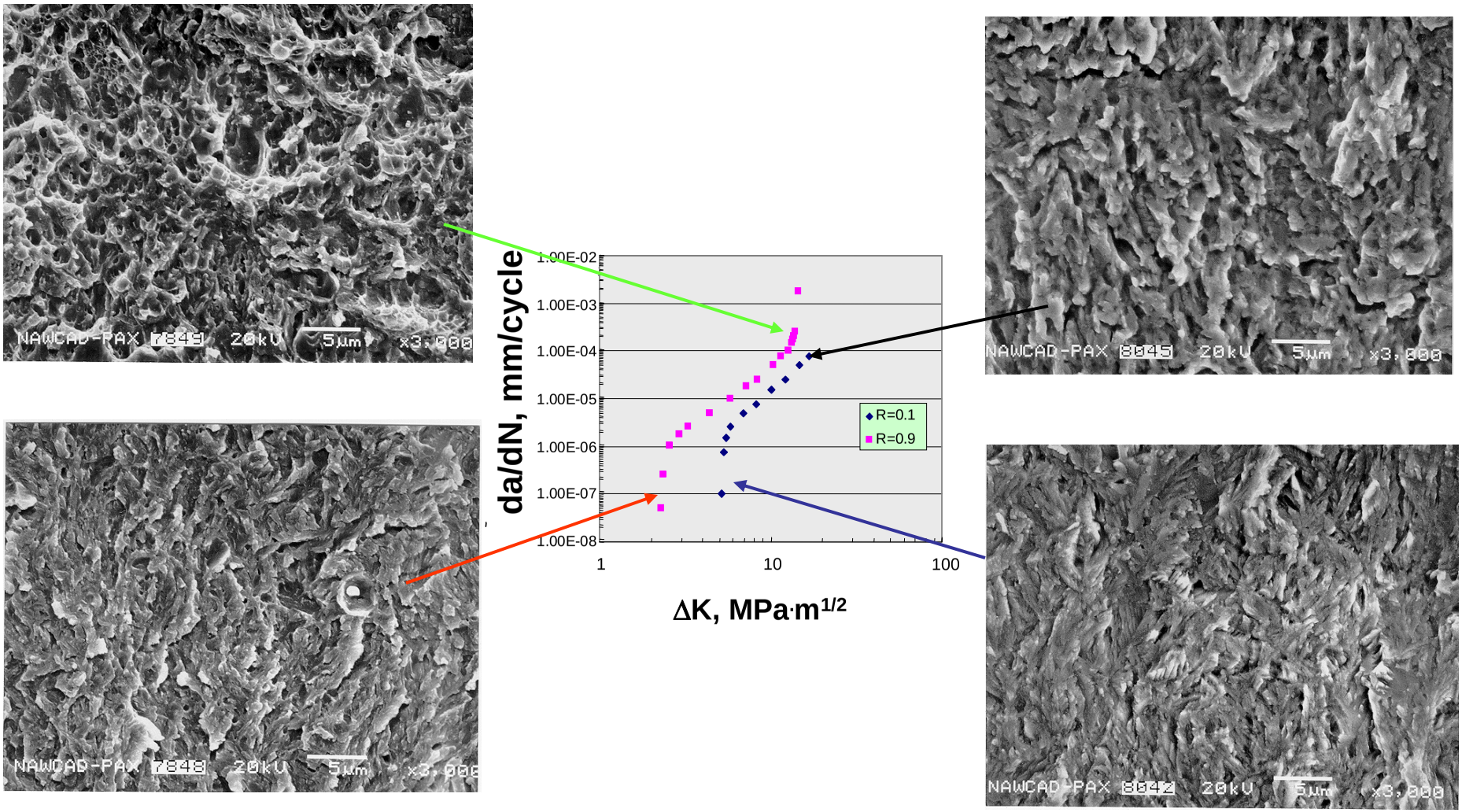

Figure A-15: da/dN versus ΔK Curves and SEM Fractographs of AerMet 100 Steel, Fatigued in Air

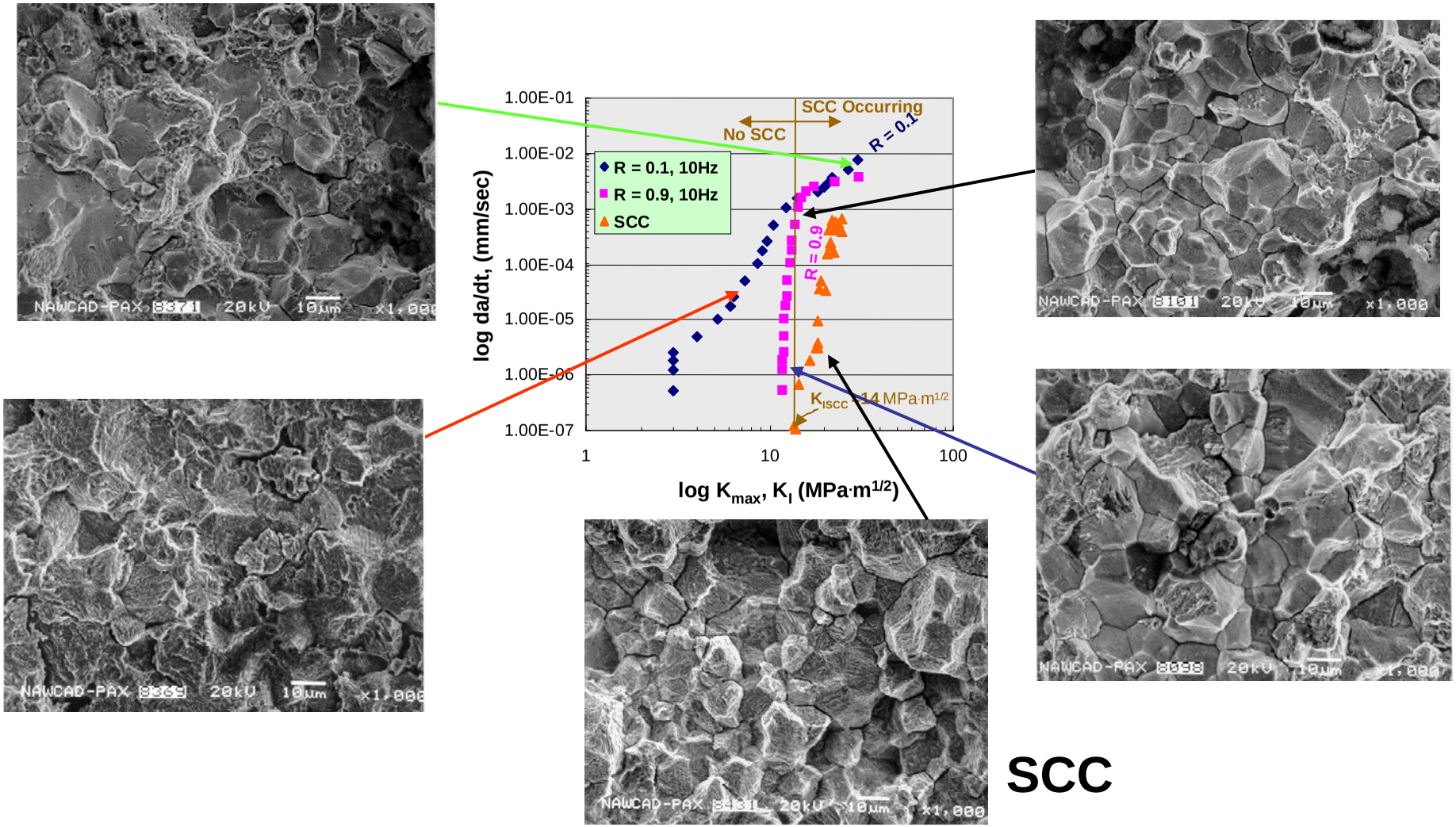

Figure A-16: da/dt versus K_{max} and K_I Curves and SEM Fractographs of 4340 Steel, Fatigued in 3.5% NaCl

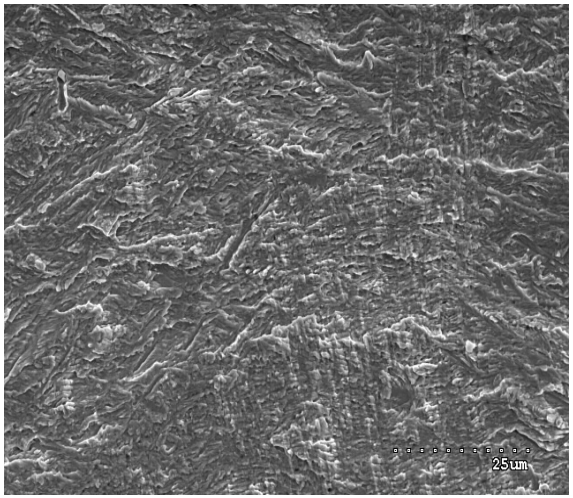

a. Regime A in Air

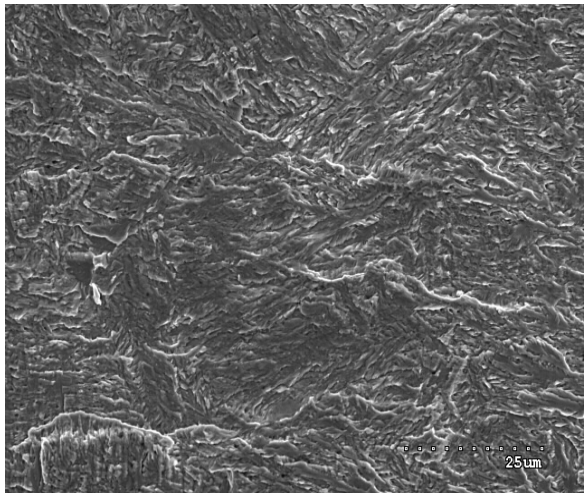

b. Regime B in Air

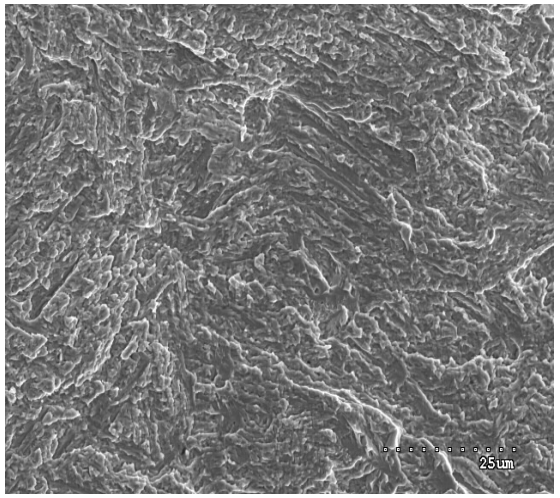

c. Regime C in Air

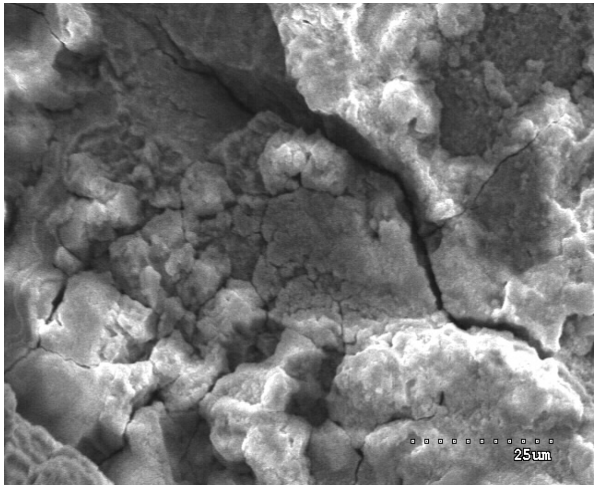

d. Regime A in 3.5% NaCl

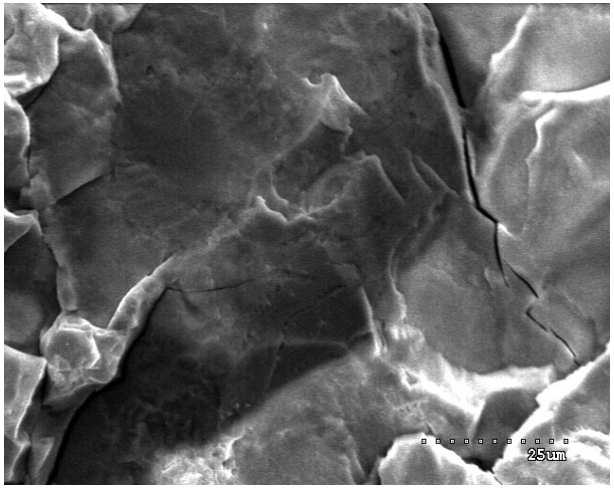

e. Regime B in 3.5% NaCl

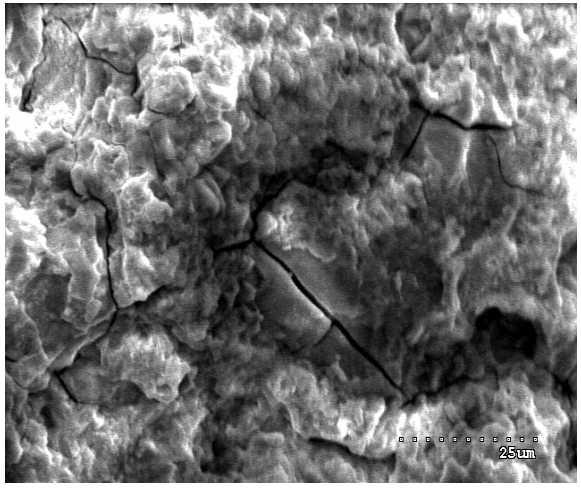

f. Regime C in 3.5% NaCl

Figure A-17: SEM Fractographs of Ferrium, Fatigued in Air and 3.5% NaCl Solution

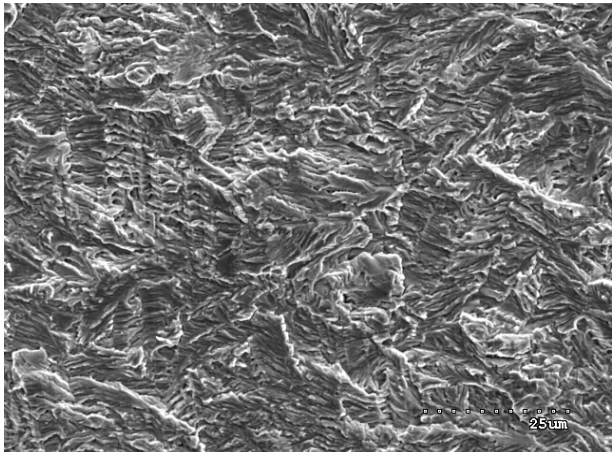

a. Regime A in Air

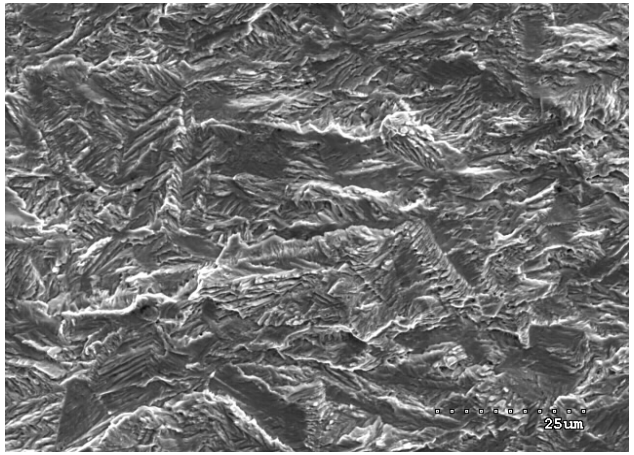

b. Regime B in Air

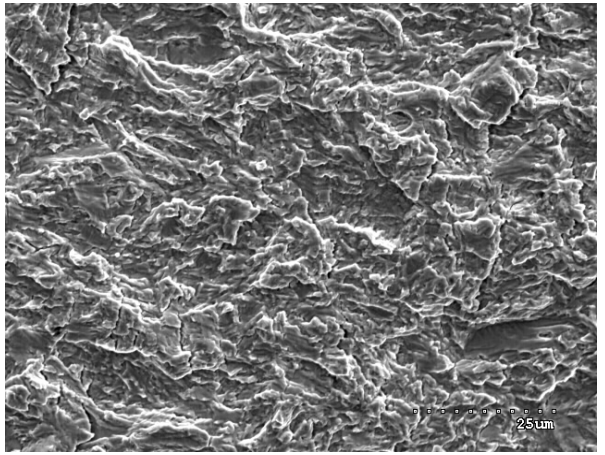

c. Regime C in Air

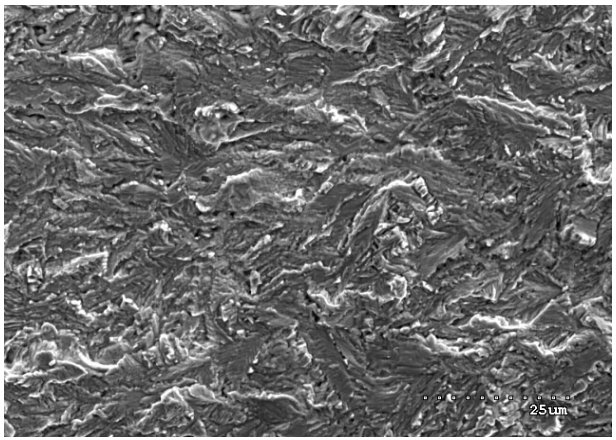

d. Regime A in 3.5% NaCl

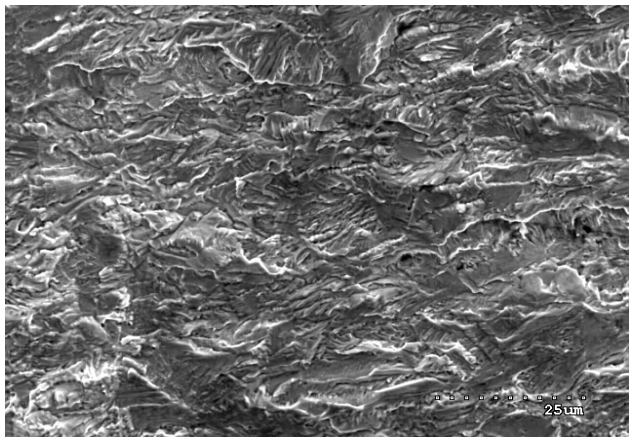

e. Regime B in 3.5% NaCl

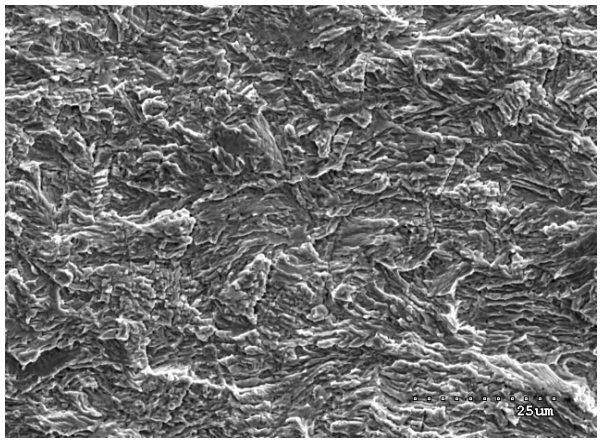

f. Regime C in 3.5% NaCl

Figure A-18: SEM Fractographs of 13-8Mo, Fatigued in Air and 3.5% NaCl Solution

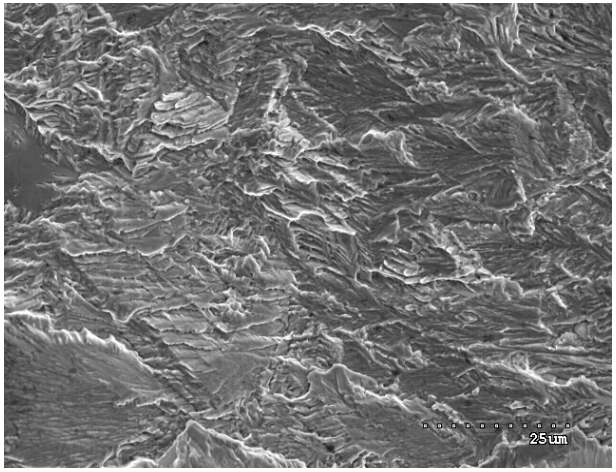

a. Regime A in Air

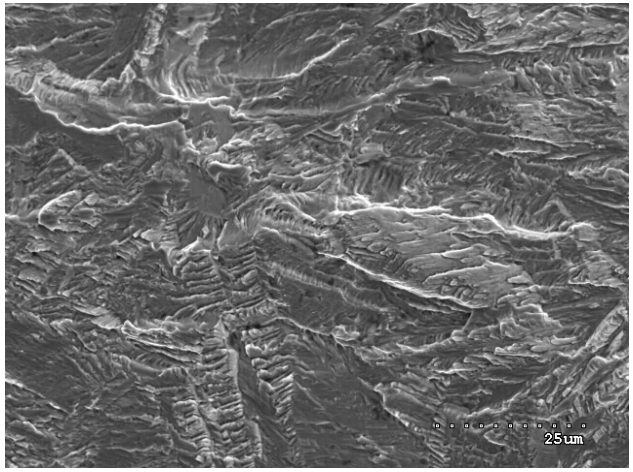

b. Regime B in Air

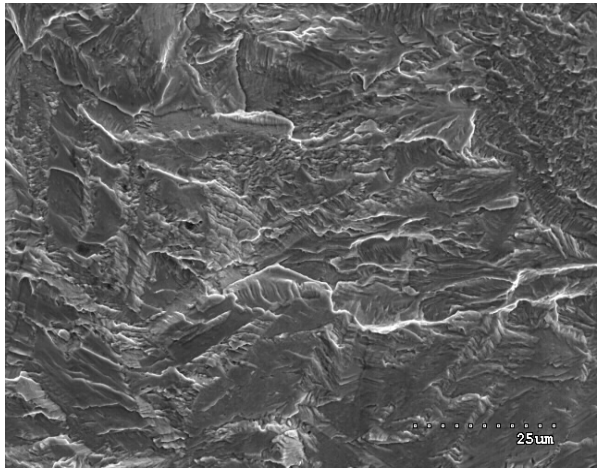

c. Regime C in Air

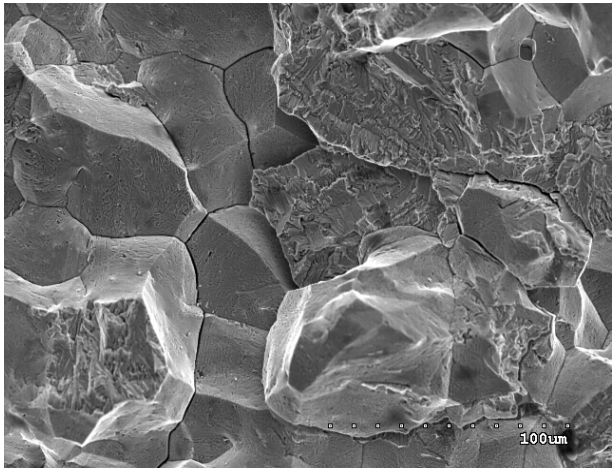

d. Regime A in 3.5% NaCl

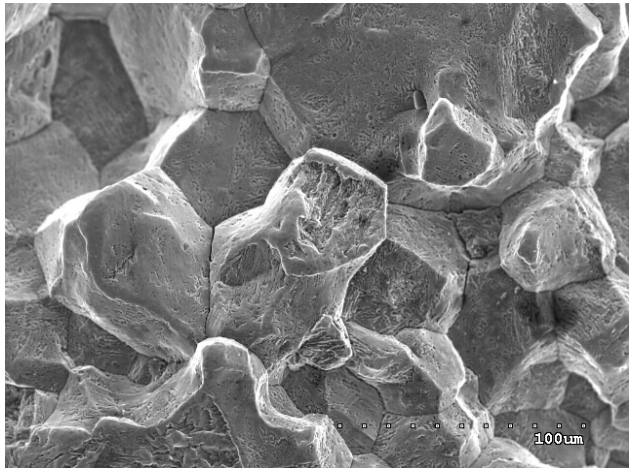

e. Regime B in 3.5% NaCl

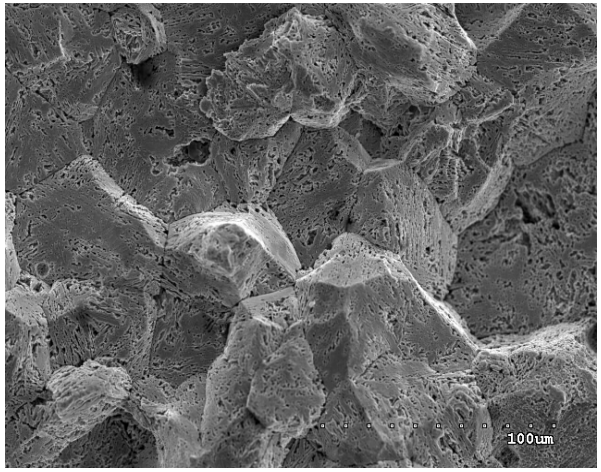

f. Regime C in 3.5% NaCl

Figure A-19: SEM Fractographs of Custom 465, Fatigued in Air and 3.5% NaCl Solution

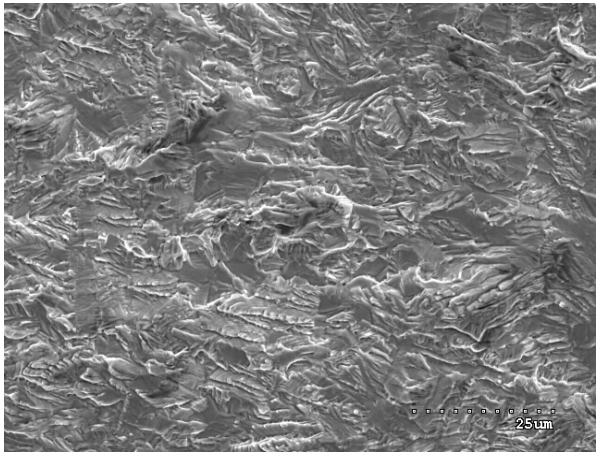

a. Regime A in Air

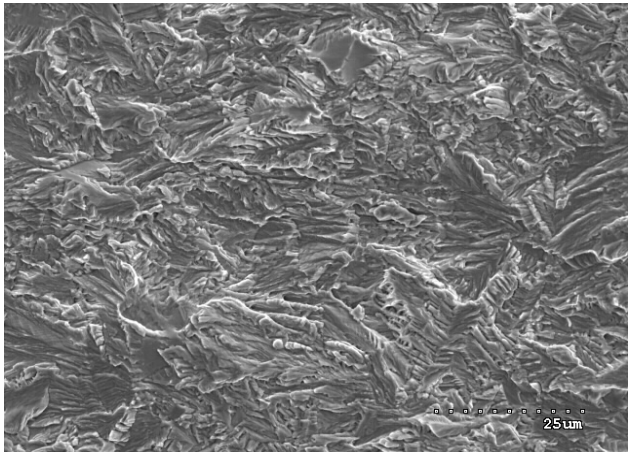

b. Regime B in Air

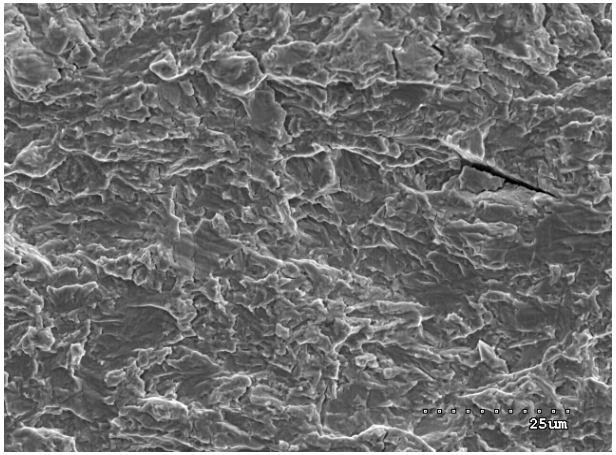

c. Regime C in Air

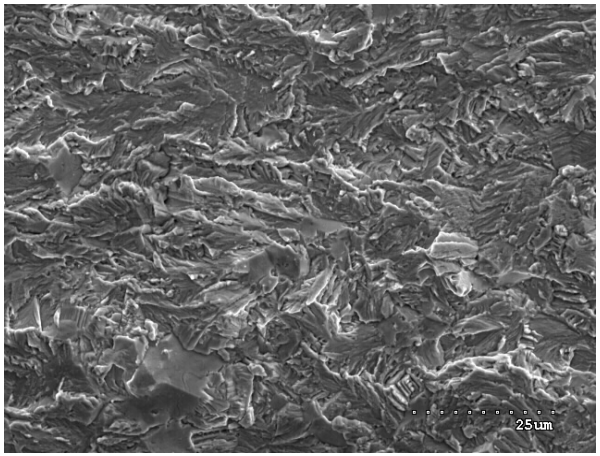

d. Regime A in 3.5% NaCl

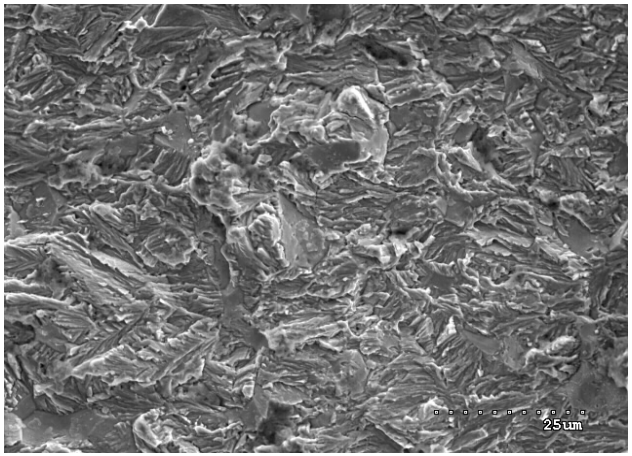

e. Regime B in 3.5% NaCl

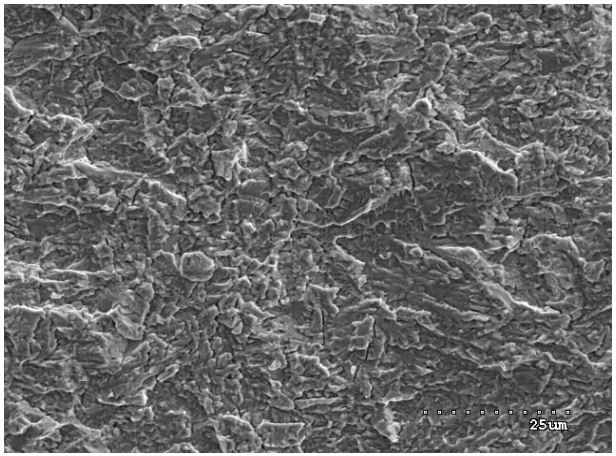

f. Regime C in 3.5% NaCl

Figure A-20: SEM Fractographs of MLX17, Fatigued in Air and 3.5% NaCl Solution

APPENDIX B
TABLES

Table B-1: Chemical Compositions of High Strength Steels

	Composition (%)				
Element	**4340**	**300M**	**AerMet**	**Ferrium**	**Hy-Tuf**
C	0.38~0.43	0.38~0.43	0.23	0.20	0.25
Mn	0.60~ 0.90	0.60~ 0.90	0.03	0.05	1.35
Si	0.15~0.35	1.45~1.80	0.03	0.05	1.50
P	- 0.015	- 0.010	0.003	< 0.001	-
S	- 0.015	- 0.010	0.0009	0.003	-
Cr	0.70~0.90	0.70~0.95	3.03	9.40	0.30
Ni	1.65~2.00	1.65~2.00	11.09	5.75	1.80
Mo	0.20~0.30	0.30~0.50	1.18	1.98	0.40
Cu	- 0.35	- 0.35	-	0.01	0.01
Co	-	-	13.44	13.80	-
V	-	-	-	-	0.29
Fe	balance	balance	balance	balance	balance

Table B-2: Chemical Compositions of Stainless Steels

	Composition (%)			
Element	**HNSS**	**13-8Mo**	**Custom 465**	**MLX17**
Ni	15.02	7.50 - 8.50	10.75 – 11.25	11.0
Cr	29.35	12.25 - 13.25	11.00 – 12.5	12.0
Al	-	-	-	1.50
Mo	1.94	2.00 - 2.50	0.75 – 1.2	2.0
Ti	-	-	-	1.50
Mn	5.96	- 0.10	0.25	-
Si	0.51	- 0.10	0.25	-
C	0.016	- 0.05	0.020	0.01
S	0.003	- 0.008	0.0100	-
P	-	- 0.010	0.0150	-
N	0.83	- 0.01	-	-
Fe	46.33	balance	balance	balance

Table B-3: Mechanical Properties of High Strength Steels

Property	4340	300M	AerMet	Ferrium	Hy-Tuf
UTS (ksi)	282	290	294	288	235
YS (ksi)	242	240	248	228	187
Hardness (R_C)	51	54	53	54	47
Elongation (%)	10	8.5	14	19	13
K_{IC} (ksi$\sqrt{in}$)	48	55	115	70	109
K_{ISCC} (ksi$\sqrt{in}$)**	13	16	23	35	27

** in 3.5% NaCl Solution of pH 7.3

Table B-4: Mechanical Properties of Stainless Steels

Property	HNSS (H1025)	13-8Mo (H1000)	Custom 465 (H1000)	MLX17
UTS (ksi)	228	215	253	248
YS (ksi)	193	207	245	243
Hardness (R_C)	48	44	48	48
K_Q (ksi$\sqrt{in}$)	49	107	99	88
K_{ISCC} (ksi $\sqrt{in}$)	∞	77	> 59	75
Elongation (%)	16	14	13	14

DISTRIBUTION:

NAVAIRSYSCOM (AIR-4.3), Bldg. 2187 (1)
48066 Shaw Road, Patuxent River, MD 20670-1906
NAVAIRSYSCOM (AIR-4.3.3), Bldg. 2187 (1)
48066 Shaw Road, Patuxent River, MD 20670-1906
NAVAIRSYSCOM (AIR-4.3.3.2), Bldg. 2187 (1)
48066 Shaw Road, Patuxent River, MD 20670-1906
NAVAIRSYSCOM (AIR-4.3.4), Bldg. 2188 (1)
48066 Shaw Road, Patuxent River, MD 20670-1908
NAVAIRSYSCOM (AIR-4.3.4.1), Bldg. 2188 (30)
48066 Shaw Road, Patuxent River, MD 20670-1908
NADEP (Code 4.3.4) (1)
Naval Air Station, Jacksonville, FL 32212
NADEP (Code 4.3.4) (1)
22 East Avenue, San Diego, CA 92135-5112
NADEP (Code 4.3.4) (1)
PSC Box 8021, Cherry Point, NC 28533-0021
NAVAIRWARCENACDIV (1)
Highway 547, Lakehurst, NJ 08733-5000
NAVAIRSYSCOM (AIR-5.1V), Bldg. 304, Room 106A (1)
22541 Millstone Road, Patuxent River, MD 20670-1606
NAVAIRSYSCOM (AIR-5.1), Bldg. 304, Room 100 (1)
22541 Millstone Road, Patuxent River, MD 20670-1606
NAVAIRWARCENACDIV (4.12.6.2), Bldg. 407, Room 116 (1)
22269 Cedar Point Road, Patuxent River, MD 20670-1120
NAVTESTWINGLANT (55TW01A), Bldg. 304, Room 200 (1)
22541 Millstone Road, Patuxent River, MD 20670-1606
DTIC (1)
Suite 0944, 8725 John J. Kingman Road, Ft. Belvoir, VA 22060-6218